Revisiting the Pierson–Moskowitz Asymptotic Limits for Fully Developed Wind Waves

JOSE HENRIQUE G. M. ALVES* AND MICHAEL L. BANNER

School of Mathematics, University of New South Wales, Sydney, New South Wales, Australia

IAN R. YOUNG

Faculty of Engineering, Computer and Mathematical Sciences, University of Adelaide, Adelaide, South Australia, Australia

(Manuscript received 7 August 2001, in final form 18 November 2002)

ABSTRACT

The time-honored topic of fully developed wind seas pioneered by Pierson and Moskowitz is revisited to review the asymptotic evolution limits of integral spectral parameters used by the modeling community in the validation of wind-wave models. Discrepancies are investigated between benchmark asymptotic limits obtained by scaling integral spectral parameters using alternative wind speeds. Using state-of-the-art wind and wave modeling technology, uncertainties in the Pierson–Moskowitz limits due to inhomogeneities in the wind fields and contamination of the original data by crossing seas and swells are also investigated. The resulting reanalyzed database is used to investigate the optimal scaling wind parameter and to refine the levels of the full-development asymptotes of nondimensional integral wave spectral parameters used by the wind-wave modeling community. The results are also discussed in relation to recent advances in quantifying wave-breaking probability of wind seas. The results show that the parameterization of integral spectral parameters and the scaling of nondimensional asymptotes as a function of U_{10} yields relations consistent with similarity theory. On the other hand, expressing integral spectral parameters and scaling nondimensional asymptotes as a function of u_* or alternative proposed scaling wind speeds yields relations that do not conform to similarity requirements as convincingly. The reanalyzed spectra are used to investigate parameter values and shapes of analytical functions representing fully developed spectra. These results support an analytical form with a spectral tail proportional to f^{-4}.

1. Introduction

It has been several decades since the publication of the seminal paper of Pierson and Moskowitz (1964, hereinafter PM64) on observations of fully developed wind seas and their parameterization. Within this time frame, there has been remarkable scientific progress in wind-wave measurement technology, highlighted by the transition from the single-point time series from ship-borne wave-height recorders, as used by PM64, to present-day two-dimensional spatially extensive sea surface topography, derived from scanning radar and lidar altimeters deployed from aircraft. On a larger scale, satellite-borne synthetic aperture radar (SAR), scatterometer, and altimetry technologies have profoundly revolutionized our observational capability for monitoring winds and waves on a planetary scale. Equally impressive are present-day predictive spectral evolution models for computing sea state and producing routine forecasts of global wind and wave climates.

The synoptic conditions that give rise to fully developed seas free of crossing wind seas and swells, currents, and unsteady winds occur relatively infrequently. Hence, since the publication of PM64, the number of studies of fully developed seas has been remarkably scant, as discussed in detail below. Yet, such fully developed sea states form an important conceptual quasi-asymptotic benchmark for assessing the stage of development of the dominant sea waves, both in routine observations and in wind-wave model validation.

This paucity of attention has also been paralleled on the theoretical side, where the modeling investigation of Komen et al. (1984, hereinafter KHH) is arguably the landmark model study. Based on the radiative transfer equation for the evolution of the directional wave action spectrum with source terms for wind input, nonlinear spectral interactions, and dissipation, KHH highlighted the need to examine carefully the underlying directionality of the wave field if the classic Pierson–Moskowitz spectrum was to be a genuine equilibrium spectrum. Interestingly, their conclusion was that a

* Current affiliation: SAIC/GSO at Marine Modeling and Analysis Branch, EMC, NOAA/NCEP, Camp Springs, Maryland.

Corresponding author address: Prof. Michael L. Banner, School of Mathematics, University of New South Wales, 2052 Sydney, Australia.
E-mail: m.banner@unsw.edu.au

JONSWAP-like spectrum (Hasselmann et al. 1973) characterized by a strongly bimodal directional tail was needed to deliver a true equilibrium frequency spectrum for full development conditions, within the constraints of their assumed source terms. However, we note that their equilibrium frequency spectrum departed considerably from the empirically based spectrum proposed subsequently by Donelan et al. (1985).

An additional fundamental issue introduced by KHH was the adoption of u_* as the reference velocity scale to replace the 19.5-m reference wind speed $U_{19.5}$ or the more familiar 10-m reference wind speed U_{10}. In replacing $U_{19.5}$ by u_* using a constant drag coefficient, however, KHH implied that these two scaling wind speeds follow a linear interrelationship. This assumption is not consistent with more recent observations that imply a wind speed dependence on the drag coefficient and, thus, a nonlinear relationship between u_* and the reference wind speed U_{10} or $U_{19.5}$. Consequently, KHH may have introduced an inconsistency that persists today because of common practice. Indeed, one of the primary motivations for the present study was to resolve potential inconsistencies by revisiting the issue of which scaling wind speed is optimal, based on a reanalysis of the PM64 data and considering their statistical significance.

Overall, from a modeling perspective the spectral structure of fully developed seas is dependent on the source terms (wind input, nonlinear spectral transfers, and dissipation). While our knowledge has progressed beyond the wind input and dissipation rate source terms used by KHH, as discussed in the recent monograph by Komen et al. (1994), sensitivity to uncertainties in these source terms arguably renders definitive theoretical work on the asymptotic directional spectrum premature at this point in time.

It should also be pointed out that there are fundamental questions as to whether full development actually exists, together with a suite of closely related unresolved issues. These include whether breaking of the dominant seas occurs and whether wave–turbulence interaction and energy flux to the atmosphere mediated by dominant waves traveling faster than the following wind act at the forward face of the spectrum to balance the small nonlinear flux from wind input to shorter scales. Observationally, relatively little new insight on full development has emerged, except for a confirmation of the plausibility of bimodality in the directional wavenumber spectral tail region, based on observed cases approaching full development (e.g., Cote et al. 1960; Holthuijsen 1983; Hwang et al. 2000).

Thus, despite the passage of several decades, the PM64 dataset occupies a special place and is still a cornerstone of wave research (e.g., see Hanson and Phillips 1999), warranting a reanalysis that draws upon modern technological hindcast tools to examine the overall context of the realizations, statistical inference techniques to examine the sampling variability, and considers the implications of the significant wave steepness in relation to recent results on wave breaking. This motivation underpins our revisit of the PM64 dataset. The extension of such a study to embrace new datasets gathered by modern wave measurement technologies remains a challenging task for the future.

2. Historical background

Field measurements of wind-wave spectra indicate that a wind field with constant speed and direction blowing homogeneously over large areas will cause the wave field to evolve until it reaches a stationary state, known as full development. Such fully developed seas are commonly described by limiting or asymptotic values of integral spectral parameters: total energy E_{tot} or significant wave height H_s and spectral peak frequency f_p. Total energy and significant wave height describe the same integral spectral property, because they are related through the expression $H_s = 4\sqrt{E_{\text{tot}}}$. However, a common practice in wind-wave research is to establish dimensional relationships between wave parameters and other environmental variables using H_s, while nondimensional formulas are usually expressed in terms of E_{tot}. This common-practice convention will be applied throughout our investigation.

a. Similarity theory formulas

Under conditions of fetch- or duration-limited growth, it is generally accepted that the wave spectrum will evolve with E_{tot} growing while f_p decreases until respective asymptotic levels are reached. At that stage the wave field and its descriptive parameters no longer depend on time or fetch but are exclusively a function of the wind speed alone. This concept is consistent with arguments based on the similarity theory of Kitaigorodskii (1962, 1973), who proposed that whenever a steady state is reached, the associated one-dimensional frequency spectrum $F(f)$ will be a universal function Φ of the nondimensional frequency $U_0 f/g$ of the form

$$\frac{F(f)g^3}{U_0^5} = \Phi\left(\frac{U_0 f}{g}\right), \tag{1}$$

where U_0 is a reference wind speed, f is the wave frequency, and g is the acceleration due to gravity. Consequently, integral spectral parameters E_{tot}, H_s, and f_p will also be functions of the wind speed only, given by

$$H_s^{\lim} = C_1 U_0^n \quad \text{or} \quad E_{\text{tot}}^{\lim} = C_2 U_0^m \quad \text{and}$$
$$f_p^{\lim} = C_3 U_0^l, \tag{2}$$

where the superscript lim refers to the asymptotic values, while $C_{1,2,3}$ are proportionality coefficients. The exponents m, n, and l are usually determined empirically. However, to attain universality and remain consistent with similarity theory, dimensional analysis requires that $m = 4$, $n = 2$, and $l = -1$, providing the nondimensional relations

TABLE 1. Reanalyzed fully developed wind-sea events from the MPM62 database. Original data have been transformed into SI units; date–time listed as two-digit ddmmyy hh (UTC; years are yy + 1900). Tabulated parameters are the 19.5-m height wind speed $U_{19.5}$, the 10-m height wind speed U_{10}^{N} corrected for atmospheric stability, the friction velocity u_*, the significant wave height H_s^{M64} as provided by M64, the percentage corrections for swell CSW and crossing seas CXS applied on reanalyzed spectra extended to $f = 0.5$ Hz to obtain the significant wave height H_s^{C}, the U_{10}-scaled nondimensional energy ϵ, and the u_*-scaled nondimensional energy ϵ_*. Events used for obtaining grouped data are indicated in the last column. Two new cases are identified by blank entries for $U_{19.5}^{M64}$ and H_s^{M64}.

Date–time		$U_{19.5}^{M64}$	U_{10}^{N}	u_*	H_s^{M64}	CSW	CXS	H_s^{C}	ϵ	ϵ_*				
ddmmyy	hh	(m s^{-1})	(m s^{-1})	(m s^{-1})	(m)	(%)	(%)	(m)	$\times 10^{3}$	$\times 10^{-3}$	f_p (Hz)	ν	$\nu_* \times 10^{3}$	Group
090455	00		21.62	0.94		1.32	0.00	11.64	3.74	1.06	0.07	0.14	6.23	
070655	18	12.35	11.68	0.43	4.05	0.77	6.50	3.70	4.43	2.31	0.10	0.12	4.56	1
070655	21	12.86	12.03	0.45	4.36	1.59	7.15	3.94	4.45	2.26	0.09	0.11	4.24	1
080655	15	12.86	12.12	0.45	3.99	3.82	8.08	3.37	3.17	1.60	0.08	0.10	3.85	
051155	03	18.00	16.91	0.69	7.44	3.38	7.81	5.77	2.45	0.90	0.09	0.16	6.42	2
051155	06	16.46	15.66	0.62	6.86	2.30	8.75	5.71	3.25	1.29	0.09	0.15	5.82	2
200356	18	14.92	14.12	0.55	6.28	1.03	0.01	6.24	5.88	2.57	0.08	0.11	4.29	3
210356	00	14.92	14.03	0.55	6.46	1.47	0.04	6.29	6.13	2.70	0.08	0.12	4.71	3
110556	21	19.55	18.31	0.76	9.48	2.27	0.00	9.26	4.59	1.55	0.07	0.13	5.24	
190656	14	10.29	9.49	0.34	2.16	0.65	0.46	2.13	3.36	2.09	0.14	0.14	4.82	
190656	18	9.77	9.66	0.35	2.41	2.24	0.39	2.43	4.10	2.51	0.13	0.13	4.73	
200656	00	10.29	10.03	0.36	2.13	0.49	0.26	2.28	3.09	1.83	0.13	0.14	4.92	
200656	03	9.26	9.64	0.34	2.04	0.64	0.09	2.23	3.47	2.13	0.14	0.13	4.76	
200656	06	9.77	9.77	0.35	2.16	1.22	0.03	2.29	3.46	2.10	0.15	0.15	5.35	
200656	09	10.29	10.24	0.37	2.20	5.61	0.01	2.20	2.65	1.54	0.14	0.14	5.13	4
200656	12	9.77	9.52	0.34	2.23	1.76	0.01	2.19	3.50	2.17	0.15	0.14	5.13	4
211156	03	21.60	20.26	0.86	10.09	5.94	0.01	9.71	3.37	1.02	0.08	0.17	7.33	
251156	03	21.60	20.16	0.86	9.63	2.26	0.00	9.28	3.13	0.95	0.07	0.13	5.69	5
251156	09	19.55	18.25	0.76	10.52	3.67	0.06	9.62	5.02	1.70	0.07	0.12	5.09	5
050358	06		19.84	0.84		1.71	0.24	9.12	3.23	1.00	0.08	0.16	6.68	
180458	06	12.35	11.95	0.45	3.51	1.12	0.43	3.40	3.40	1.73	0.11	0.14	5.13	6
180458	12	12.86	12.38	0.47	3.66	0.80	0.92	3.66	3.43	1.69	0.10	0.12	4.61	6
250458	18	18.00	17.00	0.69	7.32	1.55	0.01	7.28	3.82	1.39	0.07	0.12	4.96	
291058	09	14.92	13.99	0.54	6.07	2.06	0.00	6.03	5.71	2.52	0.08	0.12	4.60	7
291058	18	15.43	14.53	0.57	6.19	1.39	0.00	6.10	5.02	2.14	0.08	0.11	4.49	7
111258	18	18.00	16.95	0.69	6.77	1.51	0.09	6.70	3.27	1.20	0.07	0.13	5.20	
121258	06	20.58	19.33	0.81	8.96	0.76	0.01	8.92	3.43	1.09	0.05	0.10	4.33	8
121258	12	20.58	19.57	0.83	8.90	1.25	0.01	8.65	3.06	0.96	0.07	0.13	5.51	8
240159	18	16.46	15.61	0.62	6.40	0.80	1.39	6.35	4.09	1.62	0.06	0.10	3.97	

$$\epsilon^{\lim} = \frac{E_{\text{tot}}^{\lim} g^2}{U_0^4} \quad \text{or} \quad \zeta^{\lim} = \frac{H_s^{\lim} g}{U_0^2} \quad \text{and} \quad \nu^{\lim} = \frac{f_p^{\lim} U_0}{g}, \tag{3}$$

where $\epsilon^{\lim}(\zeta^{\lim})$ and $\nu^{\lim}$ are constants (for simplicity, the superscript lim will be dropped henceforth). Equations (3) define asymptotic bounds for the fetch- and duration-limited evolution of integral properties of wind wave spectra. To be consistent with similarity theory, observed wind and wave parameters have to satisfy simultaneously Eqs. (2) and (3).

b. Existing observational evidence

Several attempts have been made since the pioneering work of Sverdrup and Munk (1947) to estimate asymptotic spectra and integral parameters as a function of wind speed. Early contributions include Pierson et al. (1955), Darbyshire (1959), and the revision of Sverdrup and Munk's findings reported in Bretschneider (1966). These early studies showed strong disagreement, attributed to the poor quality of the wave data, nonstandard wind observations in respect to anemometer height, and neglect of such effects as unsteady winds, varying or moving fetches, and atmospheric stability.

With the purpose of reconciling the discrepancies found in these earlier studies, Pierson and Moskowitz published a series of three papers analyzing a carefully chosen dataset representative of fully developed seas (Moskowitz 1964, hereinafter M64; PM64; Pierson 1964). The datasets used in these studies were summarized in M64. Observations were made using shipborne wave gauges carried by oceanographic vessels at the following ocean weather stations (OWS) located in the North Atlantic Ocean: Alpha (62°N, 33°W), India (59°N, 19°W), Juliet (52.5°N, 20°W), and Kappa (45°N, 16°W).

From nearly 1000 measurements, 460 events reported by Moskowitz et al. (1962, hereinafter MPM62) were selected and analyzed by M64 on the basis of synoptic criteria applied to surface pressure charts. From these, 54 cases were retained that were apparently free of swell contamination and/or uncertainties related to the accuracy of observed local winds. Tables 1 and 2 show relevant parameters of the M64 dataset. Original values in feet, knots, and nautical miles have been converted into SI–mks units.

TABLE 2. Fully developed wind-sea events from the M64 database that failed our rejection criteria; date–times as in Table 1. Flags indicate events that were excluded as not satisfying criteria for homogeneity–stationarity of wind fields (HOST), bimodal spectra (BIMS), or crossing seas (XSEA). The description of other symbols is found in the caption of Table 1.

Date–time								
ddmmyy	hh	$U_{19.5}^{M64}$ (m s^{-1})	U_{10}^{N} (m s^{-1})	u_* (m s^{-1})	H_s^{M64} (m)	HOST	BIMS	XSEA
080655	12	13.37	12.51	0.47	4.12	F		
190955	03	10.80	10.33	0.37	2.47			F
190955	09	10.80	10.29	0.37	2.44		F	F
041155	00	14.40	13.55	0.52	5.79		F	F
051155	15	15.43	14.59	0.57	6.65			F
210356	21	20.06	18.76	0.78	9.88	F		
110556	09	20.58	19.25	0.81	10.15	F		
110556	12	21.60	20.21	0.86	10.49	F		
110556	14	21.09	19.70	0.83	10.21	F		
110556	15	20.58	19.31	0.81	9.48	F		
061156	18	17.49	16.59	0.67	6.95			F
231156	15	16.46	15.57	0.62	6.01	F		
230557	03	13.89	13.24	0.51	4.21			F
230557	06	12.86	12.11	0.45	4.09			F
200158	15	18.00	16.89	0.69	7.01		F	F
200158	21	15.43	14.83	0.58	6.13		F	F
190458	09	15.43	14.76	0.58	6.25	F		F
240458	15	18.00	16.80	0.68	7.50	F		
240458	18	18.00	16.94	0.69	7.32	F		
240458	21	18.52	17.48	0.72	7.68	F		
101258	09	20.58	19.27	0.81	9.45	F		
160159	15	11.32	11.35	0.42	2.29	F		
240159	15	16.46	15.94	0.64	5.85			F
250759	00	13.37	12.59	0.48	2.07	F	F	
021059	09	11.83	11.20	0.41	2.47	F		F
171259	21	21.09	19.72	0.83	9.60	F		F
181259	0	20.58	19.26	0.81	10.76	F		F

PM64 not only proposed universal relations for fully developed asymptotic limits, as defined by similarity theory, but also a universal analytical form for the entire one-dimensional frequency spectrum, henceforth referred to as the PM spectrum. Universal relations were obtained based on $U_{19.5}$, the wind speed measured at a height of 19.5 m, as the scaling wind speed U_0 in Eqs. (1), (2), and (3).

More recent observations of fetch- and duration-limited waves (Liu and Ross 1980; Donelan et al. 1985; Ewing and Laing 1987; Walsh et al. 1989; Donelan et al. 1992) provide support to these earlier studies and to the concept of deterministic asymptotic nondimensional limits for ϵ and ν, while other investigators suggest that the concept of full development should be rejected altogether (e.g., Glazman and Pilorz 1990; Glazman 1994). As a consequence of inconclusive evidence, the PM64 results continue to be used as a practical benchmark.

c. Wind speed scaling

A very important aspect of wind-wave growth studies concerns the most appropriate scaling wind speed U_0 in Eqs. (1), (2), and (3). Within the wave-modeling community a preference is shown toward using the friction velocity u_*, as reflected in Komen at al. (1994, sections II.8.4 and III.6.4). Observational studies supporting u_* scaling include Janssen et al. (1987) and Davidan (1996). Many experimentalists, however, criticize that choice because u_* is rarely measured directly, but is usually estimated through assumptions about the wind profile over the sea surface. Therefore, parameterized u_* estimates may introduce uncertainties that add to instrumental errors. Consequently, the routinely measured wind speed at 10-m height U_{10} has been taken as the natural scaling parameter by many investigators (e.g., Bretschneider 1966; Mitsuyasu et al. 1975; Hasselmann et al. 1973; Kahma 1981; Donelan et al. 1985, 1992; Walsh et al. 1989; Ebuchi et al. 1992; Young and Verhagen 1996).

Another possible alternative is $U_{\lambda/2}$, the wind speed at a height corresponding to one-half of the wavelength (λ) of the dominant waves, introduced by Donelan and Pierson (1987). Despite its physical appeal, there is presently no experimental evidence supporting the preferential use of $U_{\lambda/2}$. More recently Resio et al. (1999) have proposed a dynamically scaled wind speed U_r, taken at a height that is linearly related to the wavelength of the spectral peak. Evidence presented by Resio et al. (1999) in favor of U_r is based on a single dataset reported by Ewing and Laing (1987), who caution that their own measurements may not represent fully developed conditions.

A detailed comparative analysis of several fetch-limited datasets made by Kahma and Calkoen (1992) has

shown that existing observations do not provide conclusive evidence ruling out either U_{10} or u_* scaling. Both appear to produce evolution curves for integral spectral parameters that fit observations with similar error levels. However, the friction velocity u_* is related to U_{10} through

$$u_*^2 = U_{10}^2 C_D, \tag{4}$$

where C_D is the drag coefficient at a height of 10 m and for all reported parameterizations of C_D, the resulting dependence between u_* and U_{10} is nonlinear. Furthermore, the standard logarithmic wind profile for neutrally stable atmospheric conditions defined by

$$U_z = U_{10} \frac{\ln(z/z_0)}{\ln(10/z_0)} \tag{5}$$

provides expressions for $U_{\lambda/2}$ and U_r that also depend nonlinearly on U_{10}. Equations (4) and (5) imply that, if universality of Eqs. (1), (2) and, (3) holds for U_{10}, it will not hold for u_*, $U_{\lambda/2}$, and U_r or vice versa.

1) Scaling with fixed-height winds

Using observations of the wave spectrum, M64 verified that the relationship between the 54 associated values of H_s and $U_{19.5}$ selected from MPM62 could be approximated by the following expression in the form of Eq. (2), as postulated by similarity theory:

$$H_s = 0.023 U_{19.5}^2. \tag{6}$$

Aiming at a reduction of the variability in his observations, M64 averaged the 54 measured spectra into representative spectra for five $U_{19.5}$ classes: 20, 25, 30, 35, and 40 kt. PM64 then used these average spectra to derive a universal analytical expression describing the entire frequency spectrum as a function of $U_{19.5}$:

$$F(f) = \alpha g^2 (2\pi)^{-4} f^{-5} \exp\left[-1.25\left(\frac{f_m}{f}\right)^4\right], \tag{7}$$

where $F(f)$ is the frequency spectrum, $f_m = \nu_{\rm pm} g/U_{19.5}$ is the dimensional peak frequency in hertz, related to the $U_{19.5}$-scaled nondimensional peak frequency $\nu_{19.5}^{\rm pm} = 0.14$, and $\alpha = 0.0081$ is the empirically determined equilibrium range level, also known as the Phillips constant from the work of Phillips (1958) on equilibrium ranges of wind-wave spectra.

The PM spectrum of Eq. (7) was produced by fitting coefficients of an analytical expression to the nondimensional spectral densities $F(f)g^3/U_{19.5}^5$ of these five average spectra. However, the fitting was made after some reassessment of the original data since the nondimensional spectral densities scaled by the observed $U_{19.5}$ did not collapse onto one curve. PM64 attributed the discrepancies to inaccuracies in the wind measurements. They overcame this difficulty by rescaling the observed $U_{19.5}$ wind speeds with a factor that forced the average nondimensional peak spectral densities to a common value. As a result of rescaling with these corrected $U_{19.5}$, their five nondimensional average spectra ($U_{19.5}$ spectra) then collapsed approximately onto a single curve.

M64 recomputed the relation between H_s and U_{10} in Eq. (6) by integrating the analytical PM spectrum. He justified this procedure on the basis of unreliable spectral estimates at frequencies higher than 0.25 Hz due to limitations in the wave recorder that may have distorted the estimates of H_s used in Eq. (6). Despite the fact that the analytical form would give only an approximation to spectral densities in the energy-containing ranges, he argued that it would minimize measurement errors in the high-frequency region, assuming that energy densities within this spectral range conformed to an f^{-5} power law. More recent observations, however, indicate that a proportionality of the spectral tail to f^{-4} is more likely in this spectral subrange.

Integration of the PM spectrum resulted in the following expression:

$$H_s = 0.021 U_{19.5}^2. \tag{8}$$

Using Eq. (8) instead of Eq. (6) leads to a reduction of about 10% in the estimated H_s and of around 20% in the estimated total energy for a given $U_{19.5}$. Equation (8) may be converted directly into the associated nondimensional total energy asymptote ϵ. By assuming a logarithmic wind profile given by Eq. (5) and using the drag coefficient relation proposed by Wu (1982) (see below), $U_{19.5}$ may be replaced by U_{10}, yielding

$$\epsilon_{\rm pm}^{\rm an} = \frac{E_{\rm pm}^{\rm an} g^2}{U_{10}^4} = 3.64 \times 10^{-3}, \tag{9}$$

where the superscript an refers to a value derived from integration of the analytical spectrum. Alternatively Eq. (6) gives

$$\epsilon_{\rm pm}^{\rm obs} = \frac{E_{\rm pm}^{\rm obs} g^2}{U_{10}^4} = 4.24 \times 10^{-3}, \tag{10}$$

where the superscript obs refers to a value derived from the observations.

Asymptotic values for the peak frequency $f_{\rm pm}$ were estimated by PM64 through direct averaging of the 54 spectra selected by M64, giving

$$f_{\rm pm} = 0.14 \frac{g}{U_{19.5}}, \tag{11}$$

which converts into the following relation for the nondimensional peak frequency $\nu_{\rm pm}$:

$$\nu_{\rm pm}^{\rm obs} = \frac{f_{\rm pm} U_{10}}{g} = 0.13. \tag{12}$$

Since $\nu_{\rm pm}^{\rm obs}$ was one of the parameters used by PM64 in the derivation of the analytical PM spectrum, $\nu_{\rm pm}^{\rm obs}$ and $\nu_{\rm pm}^{\rm an}$ are identical.

2) FRICTION VELOCITY SCALING

Nondimensional asymptotic limits may also be obtained by scaling the wave spectra with the friction velocity u_*. Following the framework proposed in SWAMP (1985), KHH provided expressions that are now widely used as benchmarks for validation of numerical models (e.g., Banner and Young 1994; Komen et al. 1994; Ris 1997; Schneggenburger 1998; Hersbach 1998). However, it is important to note that KHH used an estimated u_* computed from the single value $U_{10} = 15$ m s^{-1}, implying a constant drag coefficient $C_D = 1.8 \times 10^{-3}$ that was extrapolated for converting a range of arbitrary values of U_{10} into u_*.

With $U_{10} = 15$ m s^{-1}, Eq. (4) gives $u_* = 0.6364$ m s^{-1}. Using this quantity in association with values for the total energy $E_{\rm pm}$ and peak frequency $f_{\rm pm}$ obtained from the integration of Eq. (7), KHH proposed the following values for u_*-scaled nondimensional asymptotic limits:

$$\epsilon^{\rm an}_{{\rm pm}*} = \frac{g^2 F_{\rm pm}}{u_*^4} = 1.1 \times 10^3 \quad \text{and} \tag{13}$$

$$\nu^{\rm an}_{{\rm pm}*} = \frac{f_{\rm pm} u_*}{g} = 5.6 \times 10^{-3}. \tag{14}$$

According to the similarity theory of Kitaigorodskii (1962, 1973), the nondimensional parameters given by Eqs. (10)–(14) should be universal constants. As such, they should hold for any given values of the scaling wind speed. The analytical PM spectrum, however, was designed to provide a universal spectral form as a function of $U_{19.5}$. Universality still holds when employing a U_{10} derived from a logarithmic approximation of the wind profile since the differences between $U_{19.5}$ and U_{10} are generally small (around 7%).

The dependence of u_* on the wind speed at a fixed height, however, is given by Eq. (4), with a drag coefficient that is a nonlinear function of the chosen fixed-height wind speed. Therefore, scaling the PM spectrum with u_* for different values of U_{10} or $U_{19.5}$ using a more realistic empirical formula for the drag coefficient rather than simply taking a constant C_D, will produce nondimensional spectra (and corresponding integral parameters ϵ_* and ν_*) that are not universal constants. The numerical example below illustrates this issue.

Integration of the PM spectrum (7) gives $E_{\rm pm} = 0.2\alpha g^2 (2\pi f_m)^{-4}$, where $f_m = 0.13 g/U_{10}$ and the Phillips constant $\alpha = 0.0081$. Choosing $U_{10} =$ (5, 10, 15, 20, and 25) m s^{-1} results in $E_{\rm pm} =$ (0.02, 0.38, 1.91, 6.05, and 14.77) m^2. After introduction of these quantities into the left-hand side of Eqs. (9) and (12) the nondimensional total energy and peak frequency values all converge to $\epsilon_{\rm pm} = 3.64 \times 10^{-3}$ and $\nu_{\rm pm} = 0.13$, respectively.

Estimating u_* from U_{10} using Eq. (4) and the C_D parameterization proposed by Wu (1982), $C_D = (0.8 + 0.065 U_{10}) \times 10^{-3}$, which was based on a composite data of open-ocean measurements, gives $u_* =$ (0.1677, 0.3808, 0.6320, 0.9165, and 1.2311) m s^{-1}. Introducing these u_* into the left-hand sides of Eqs. (13) and (14) gives $\epsilon_* =$ (2.9, 1.7, 1.1, 0.8, and 0.6) $\times 10^3$ and $\nu_* =$ (4.4, 5.0, 5.6, 6.0, and 6.4) $\times 10^{-3}$. The ranges of variability of these estimates, which should instead be equal to constant values for $\epsilon^{\rm an}_{{\rm pm}*}$ and $\nu^{\rm an}_{{\rm pm}*}$, are more than (+150%, −50%) and (±15%), respectively.

The resulting differences between these u_*-scaled quantities for $\epsilon^{\rm an}_{{\rm pm}*}$ and $\nu^{\rm an}_{{\rm pm}*}$ are too large to be neglected, indicating that if scaling with U_{10} (or $U_{19.5}$) is correct, as proposed by Pierson and Moskowitz, universality may not hold for nondimensional spectral parameters scaled by u_*. Alternatively, if u_* is in fact the correct scaling wind speed, the differences found above would indicate that the nondimensional PM spectrum [Eq. (7)] and the corresponding asymptotic limits in terms of $U_{19.5}$ or U_{10} are not universal quantities.

3. Reanalysis of the PM64 database

In this section, an attempt is made to investigate the discrepancies identified above in more detail. Our strategy is to first assess the uncertainty in the M64 dataset using hindcast data produced by numerical wind and wave models. This approach is used to (i) eliminate events with atmospheric conditions not satisfying minimum synoptic criteria or with evidence of contamination by swell or crossing wind seas and (ii) identify and subtract the background swell energy present in the remaining fully developed sea events.

The next step is then to use this reanalyzed dataset to investigate the validity of Eqs. (2) and (3) using different scaling winds, to recalculate the full development asymptotes and to verify which existing analytical spectral form is supported by this reanalyzed data. The investigation described below is based on the analysis of integral spectral parameters and wind conditions derived directly from measured data, in the spirit of the reanalysis of JONSWAP data by Kahma and Calkoen (1992).

Since a complete reanalysis of the original Pierson and Moskowitz data is made, values of U_{10} and u_* are derived directly from observations of $U_{19.5}$ from a series of technical reports published by MPM62, which provide a complete description of the 460 wave spectra and other associated environmental variables used by M64 and PM64. The data were kindly made available through hard copies of the MPM62 reports provided by W. J. Pierson.

Values of u_* were calculated using a model for the atmospheric boundary layer (ABL) from Liu et al. (1979) and Liu and Tang (1996). Corrections for atmospheric stability were made using measurements of $\Delta T = T_a -$ SST provided by M64. Values of sea surface temperature (SST), relative humidity, and surface pressure were interpolated from the National Centers for Environmental Prediction (NCEP)–National Center for

Atmospheric Research (NCAR) reanalysis database (Kalnay et al. 1996) into the position and time of selected observations. Values of the air temperature T_a were estimated by adding the observed ΔT to the NCEP–NCAR SST.

a. Reassessment of synoptic wind fields

A reassessment of synoptic surface winds during the events chosen by M64 was based on atmospheric model hindcasts available from the NCEP–NCAR reanalysis database. Surface winds at a 10-m height preceding each event were screened according to criteria expected to be met for the occurrence of fully developed seas. Qualitatively, these criteria require that the wind fields should be homogeneous and quasi stationary along a minimum fetch $X_{\min}$ during a minimum duration $t_{\min}$, both functions of the wind speed. We assumed that these conditions were met whenever wind velocities did not vary by more than $\pm 15\%$ in magnitude and $\pm 20°$ in direction, for given $X_{\min}$ and $t_{\min}$.

Several conflicting values for $X_{\min}$ are found in the literature (Pierson et al. 1955; Darbyshire 1959; M64; Bretschneider 1966; Silvester 1974). To circumvent this problem, more consistent estimates of $X_{\min}$ were obtained by extrapolating the fetch-limited evolution curve of f_p proposed by Kahma and Calkoen (1992). Here $X_{\min}$ was defined as the fetch length at which the evolution curve crossed the PM64 nondimensional asymptotic level $f_p U_{10}/g = 0.13$. Minimum durations $t_{\min}$ associated with these extrapolated values of $X_{\min}$ were then estimated from the empirical formula proposed in CERC (1984):

$$\frac{t_{\min} g}{U_{10}} = 68.8 \left(\frac{X_{\min} g}{U_{10}^2} \right)^{0.67}. \tag{15}$$

NCEP–NCAR winds over the North Atlantic Ocean during periods up to 48 h preceding each fully developed sea event were searched for conditions satisfying our synoptic criteria for quasi stationarity using a computational algorithm. Whenever patches of quasi-stationary winds were found near the observation sites, rectangular areas with alongwind dimensions satisfying $X_{\min}$ were then searched for homogeneous wind conditions. An example of this procedure is given in Fig. 1.

From the 54 cases originally chosen by PM64, 14 cases did not meet our quasi-stationarity criteria; that is, no patches with quasi-stationary winds were found near the measurement site. Events with nonstationary winds were found in wind classes centered at 20 (1500 UTC 16 January and 0000 25 July 1959), 30 (1500 23 November 1956), 35 (1500, 1800, and 2100 24 April 1958), and 40 kt (2100 21 March and 0900, 1200, 1400, and 1500 11 May 1956; 0900 10 December 1958; 2100 17 December and 0000 18 December 1959). Two events observed at 0900 UTC 2 October 1959 (20-kt class) and 0900 19 April 1958 (30-kt class) passed the quasi-stationarity criteria but failed when homogeneous winds were searched within rectangles with sides greater or equal to $X_{\min}$.

Except in four cases, the vast majority of events used by PM64 that failed our quasi-stationarity test belongs to classes centered at high wind speeds ($U_{19.5} \geq 35$ kt). Nine cases come from the class centered at 40 kt alone, leaving it with five cases. The class centered at 35 kt is reduced to five cases. These findings indicate that most of the high–wind speed events selected in M64 were not fully developed, leading to a reduction of the original database from 54 to 38 events, that is; two-thirds of its original size.

M64 applied his synoptic criteria after estimating wind fetches from surface pressure charts. Since our approach is in principle different from his, we decided to search for other potential fully developed seas events within the period of interest (1955–59) using the NCEP–NCAR data. Our reanalysis of synoptic conditions, however, was limited to the dates and times associated with the 460 events reported by MPM62 since these were associated with the only measurements of wave spectra available for our study.

The complete synoptic history of atmospheric conditions associated with the 460 cases was analyzed manually for quasi stationarity and homogeneity. Apart from the 38 spectra chosen from the 54 cases studied in M64, surface winds from only two other events passed our quasistationarity and homogeneity criteria. These two new cases are included in Table 1.

b. Contamination by crossing seas

Wave spectra used in the derivation of asymptotic limits for wave growth should be free of contamination by crossing seas, secondary high-frequency wave systems, or low-frequency swell. The removal of low-frequency swell is straightforward when a well-defined separation scale is present that differentiates these systems from locally generated seas. For a small database of only 40 spectra, the removal of background energy levels associated with low-frequency swell may, therefore, be made manually by imposing a cutoff frequency at a suitable separation scale. Removal of multipeaked spectra also follows well-known procedures, as discussed below.

In principle, direct identification and removal or correction for the contamination by crossing seas of events reported by MPM62 would not be possible, because measured one-dimensional frequency spectra do not provide any information about the directional properties of the wave field. To overcome this limitation, we use an indirect approach that allows the recovery of directional properties of the wave field. This consists of generating hindcast two-dimensional wave spectra using a numerical wind-wave model forced with wind fields corresponding to the period of observations available from the NCEP–NCAR reanalysis database.

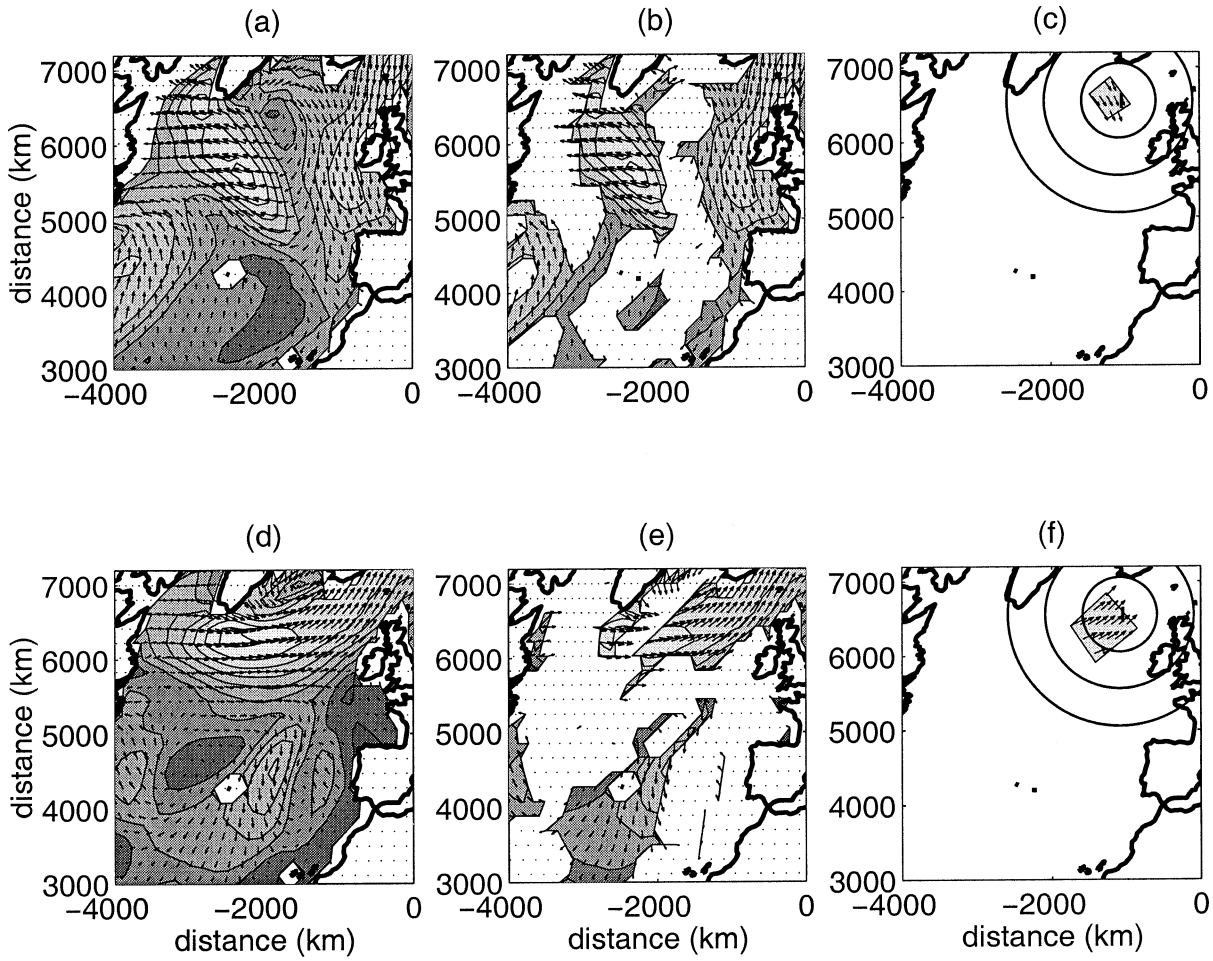

FIG. 1. Diagrams illustrating the method for identifying quasi-stationary and quasi-homogeneous surface wind fields using NCEP–NCAR reanalysis data. Contours indicate wind speeds from 2 to 16 m s^{-1} at 2 m s^{-1} intervals. (a), (d) The complete surface wind fields and vectors indicating the local wind directions over the North Atlantic Ocean. (b), (e) Quasi-stationary patches averaged over 36 h prior to 0600 UTC 9 Mar and 0600 29 Oct 1958. (c), (f) Quasi-homogeneous winds within rectangular fetches with alongwind length greater or equal to the minimum fetch X_{min}.

This modeling procedure may seem a redundant effort, since wind-wave models are usually tuned to reproduce the PM spectrum's energy levels in asymptotic-growth conditions. However, we should stress that in our investigation the simulated spectra are used exclusively to provide an estimate of the directional distribution of wave energy, information that was not previously available from the original MPM62 database of measured one-dimensional spectra.

Fulfilling the objective of obtaining accurate estimates of the directional distribution of wave spectra requires the use of forcing wind fields with realistic directional properties. For this purpose, we selected surface winds from the NCEP–NCAR reanalysis database. An assessment of the quality of these reanalysis wind directions was made possible by the availability of visual and instrumental observations of wind direction at OWS India and Juliet, provided by the British Oceanographic Data Centre (BODC, http://www.bodc.ac.uk). Although much of this data have been assimilated into the reanalysis database, it is of interest to verify the quality of the resulting NCEP–NCAR atmospheric model simulations at two sites where wave spectra reported in MPM62 were measured.

1) ASSESSMENT OF NCEP–NCAR WINDS

A comparison of NCEP–NCAR reanalyzed wind directions against 26 435 collocated observations available from OWS India (13 263) and Juliet (13 172) between 9 April 1955 and 18 December 1959 is shown in Fig. 2a. Because of the large number of collocated data points, contours of collocation density at each point from a 10° by 10° grid are presented. The agreement between NCEP–NCAR wind directions and observations is remarkably good. The NCEP–NCAR wind directions are biased by −6.26° at OWS India and by −5.56° at OWS Juliet. A linear least squares regression

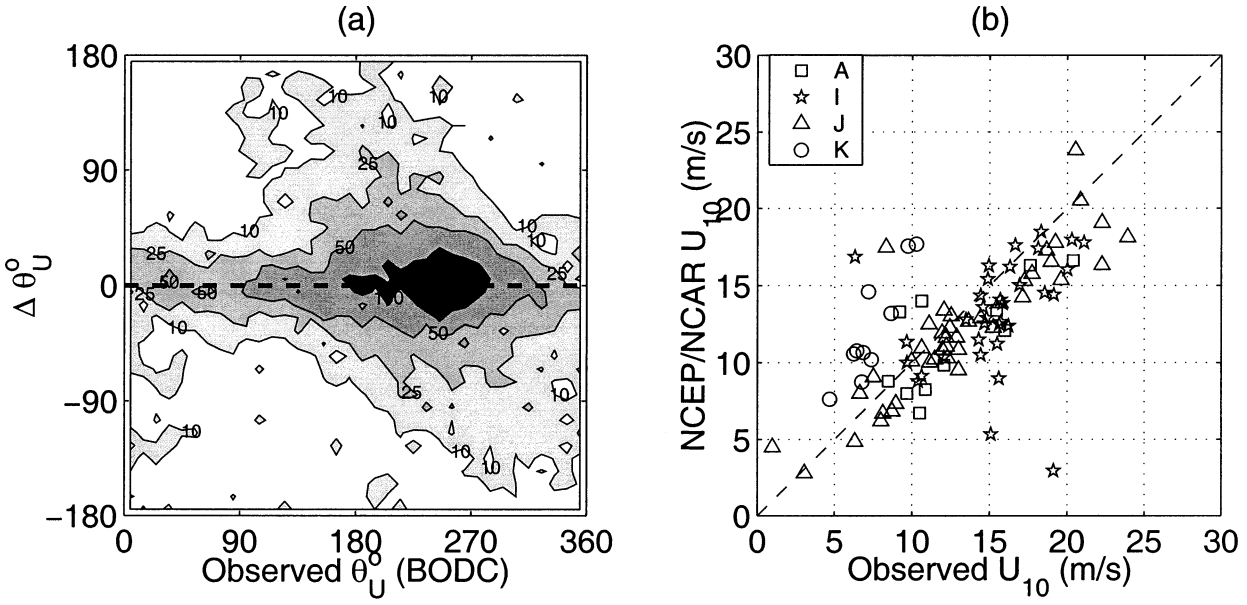

FIG. 2. Scatterplots of observed vs NCEP–NCAR reanalyzed surface wind properties: (a) directional bias $\Delta\theta_U = \theta_U^{\text{NCEP}} - \theta_U^{\text{BODC}}$ and (b) daily mean speeds U_{10}. Comparisons of θ_U were made using data from the BODC collected at OWS India and Juliet. Observed values of U_{10} were derived from MPM62 at OWS Alpha (A), India (I), Juliet (J), and Kappa (K). Because of the large number of collocated data points in (a), contours of collocation density in absolute numbers are shown.

through the cloud of collocated data gives a slope $m = 0.97$ at both observation sites.

Although of secondary importance to our analysis of directional properties of wave spectra, it is also desirable to force the wave model with wind speeds consistent with observations. The majority of observed wind speeds in the BODC database during the period of interest were visual estimates based on the Beaufort scale made by oceanographic or merchant vessels. The use of visual estimates of wind speed for the validation of atmospheric model winds is questionable because of several sources of errors and uncertainties (e.g., Lindau 1995). Our assessment of NCEP–NCAR wind speed was, therefore, made against a database of 426 wind speed measurements made by anemometers on board ships at four locations, taken from the database reported in MPM62.

Wind speed comparisons are shown in Fig. 2b. Despite a clear trend of NCEP–NCAR reanalysis data toward an underestimation of observed wind speeds by around 13%, as indicated by a regression line with slope $m = 0.87$, statistical parameter values associated with collocated data (bias $= -1.19$ m s^{-1}, rms error $\epsilon_{\text{rms}} = 4.55$ m s^{-1}, scatter index SI $= 0.31$, and correlation coefficient $r = 0.62$) indicate a generally consistent agreement between model and observed wind speeds. Although corrections for such trends would be possible, they were not pursued because the level of agreement was considered sufficient for our present purpose of estimating not the wave spectral energy densities, but solely the directional properties associated with measured one-dimensional wave spectra.

2) VALIDATION OF THE WAVE MODEL

A reconstruction of two-dimensional wave spectra was made with the third-generation wind-wave model ''WAVEWATCH III'' (Tolman 1999), with a spatial grid extending over the entire Atlantic Ocean, as illustrated in Fig. 3. This configuration allowed a representation of swell propagating from both the North and South Atlantic into the measurement sites, OWSs Alpha, India, Juliet, and Kappa, also indicated in Fig. 3. The spatial grid was bounded within 85°W to 20°E of longitude and 77°S to 77°N of latitude, with spatial resolution at 1.75° by 1.75°. The wave spectral grid used in the simulation had the minimum frequency set at $f_0 = 0.0418$, with 25 logarithmically spaced frequency bins with a separation ratio of 1.1 ($f_{\text{max}} = 0.4114$), and 24 directions with a resolution of 15°.

The model output consisted of simulated wave spectra at 3-h intervals interpolated at the positions of OWS Alpha, India, Juliet, and Kappa. Values of significant wave height H_s and mean frequency $\overline{f}$ were obtained from integration and averaging of output spectra, following the standard definitions adopted in WAVEWATCH III. A quality assessment of wave model hindcast parameters was made against observations of one-dimensional frequency spectra from the MPM62 database. Observed spectra were truncated at $f = 0.25$ Hz because of uncertainties above this cutoff frequency inherent to the recording device, and a parametric spectral tail proportional to f^{-4} was included from that frequency up to $f_{\text{max}} = 1$ Hz. The resulting spectra were then used for calculating the observed H_s and $\overline{f}$.

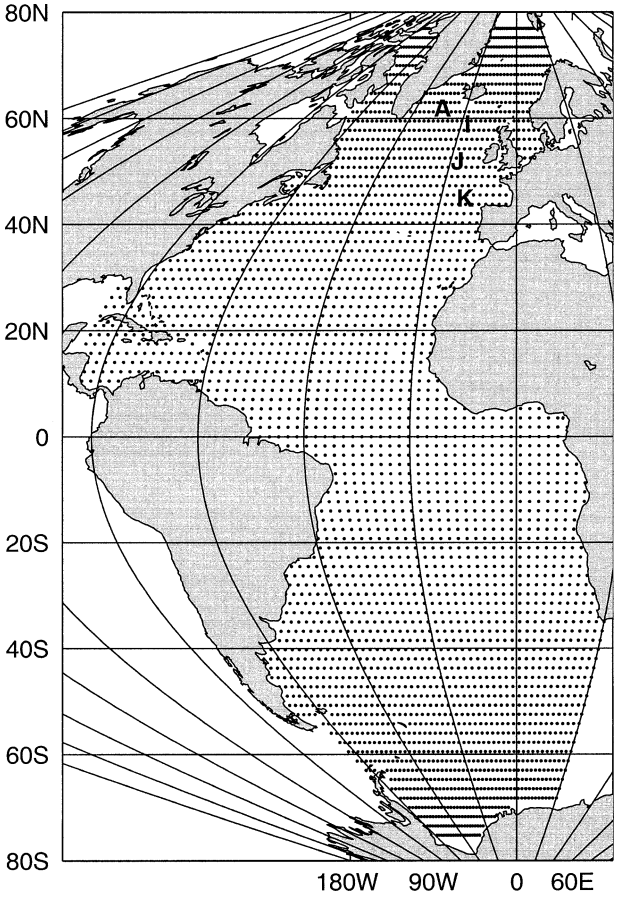

FIG. 3. Spatial grid used in the numerical simulations made with WAVEWATCH III. The locations of the observations sites Alpha (A), India (I), Juliet (J), and Kappa (K) are shown.

Figures 4a and 4b show scatterplots of collocated H_s and $\overline{f}$, respectively. Associated validation statistics for hindcast H_s were bias = −0.42 m, ϵ_{rms} = 1.72 m, SI = 0.30, and r = 0.84; for $\overline{f}$ these values were bias = −0.01 Hz, ϵ_{rms} = 0.02 Hz, SI = 0.14, and r = 0.66. Although producing small negative biases in hindcast H_s and $\overline{f}$ of under 10%, these statistics show that the computed wave fields provide spectra that are generally consistent with observations in terms of both (i) the total amount of energy carried by waves and (ii) the mean distribution of energy density within frequency bands.

Although the results shown in Fig. 4 are not completely unexpected, since the wave model used was tuned to provide asymptotic wave spectra matching the target PM64 analytical spectrum, it is reassuring that the agreement was acceptable not only in the 54 cases used in the derivation of the PM spectrum, but extended well into the other 406 cases discarded in the analysis of PM64 (i.e., the simulations reproduced well wave fields that were either not fully developed or were coexisting with crossing and swell wave fields). We assume these levels of agreement are satisfactory between simulated and observed integral wave spectral properties. Nevertheless, since our primary interest is to reconstruct the directional properties of the two-dimensional wave spectrum, a more detailed evaluation of the estimated directional energy spreading produced by the wave hindcast is presented below.

The quality of the directional properties of hindcast model spectra was assessed by comparing the calculated mean spectral wave direction θ_m with visual estimates of wave directions made by ships of opportunity obtained from the BODC. Since these data were not as-

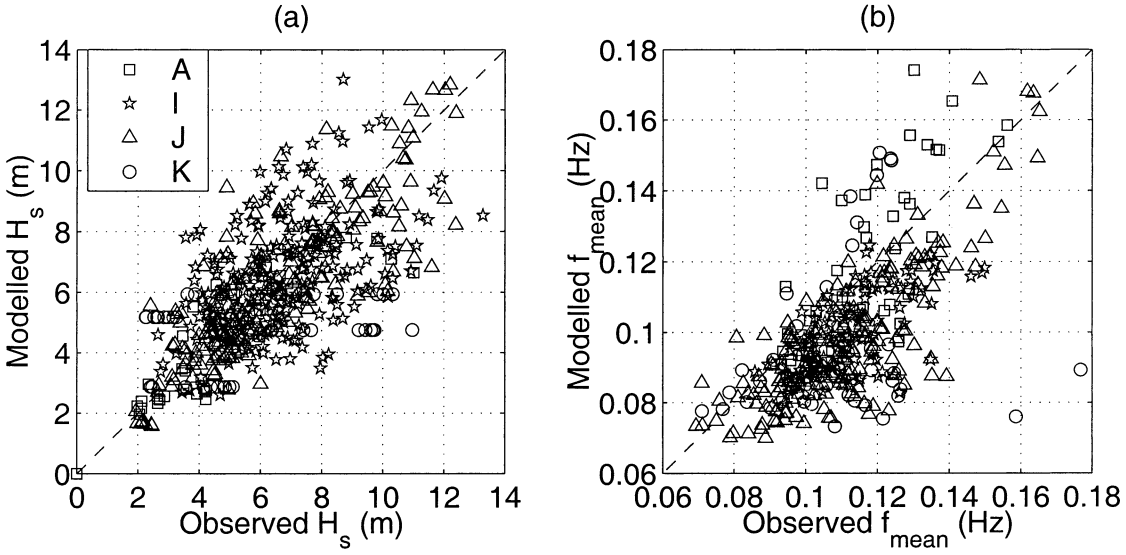

FIG. 4. Scatterplots of observed vs calculated (a) significant wave height H_s and (b) peak periods T_p. Comparisons of H_s and T_p were made using collocated data derived after integration of one-dimensional frequency spectra reported in MPM62 at OWS Alpha, India, Juliet, and Kappa.

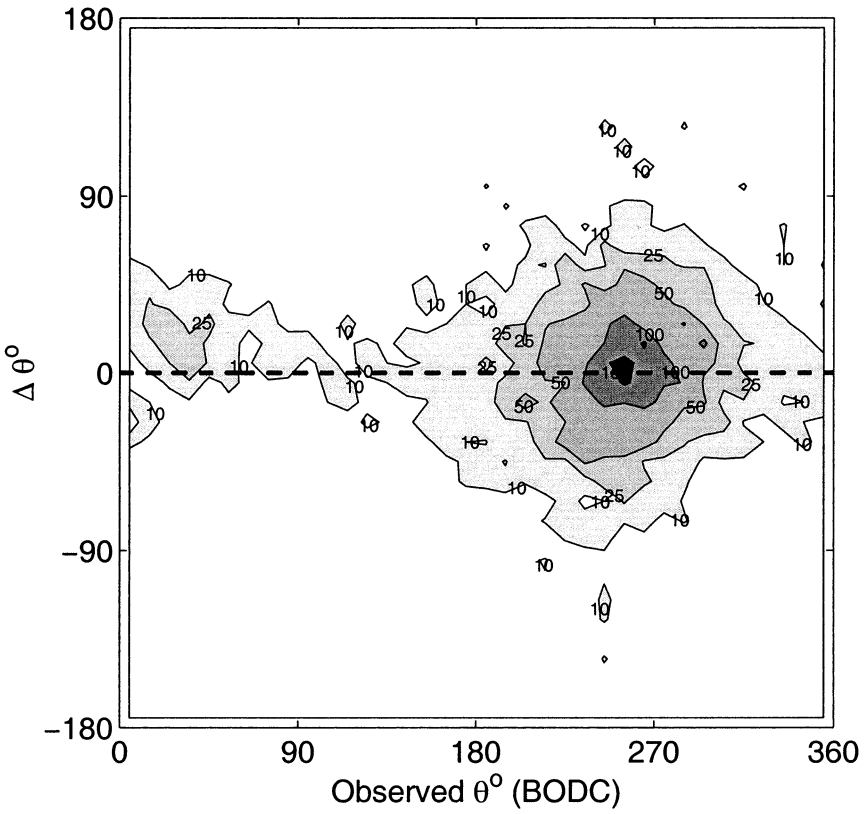

FIG. 5. Scatterplot of wave direction bias $\Delta\theta = \theta^{WW3} - \theta^{BODC}$. Comparisons were made using data from the BODC collected at OWS India and Juliet. Because of the large number of collocated data points, the scatter diagram is shown as contours of equal numbers of observations.

similated in the NCEP–NCAR reanalysis, it also provided an opportunity of verifying independently the quality of the reanalysis model surface winds used in our simulations.

Figure 5 shows a comparison of hindcast θ_m against 12 621 collocated visual estimates of wave direction available from OWS India (5647) and Juliet (6974) between 9 April 1955 and 18 December 1959. Because of the large number of collocated data points, the scatter diagram is shown as contours of equal numbers of observations at each 10° by 10° directional grid point. Hindcast values of θ_m have a negative bias of around 10° relative to visual estimates of wave direction, which is smaller than the directional resolution of the wave model used in our simulations. We conclude that the wave model provides consistent predictions of θ_m and that the quality of hindcast wave spectra is appropriate for the reconstruction of directional distributions associated with observations from the MPM62/M64 database.

3) ANALYSIS OF CROSSING SEAS

The occurrence of crossing seas in the open ocean is usually associated with sudden changes in wind direction caused by the passage of frontal systems or the arrival of swell. Whenever such wave systems are superposed on locally generated wind seas, accurate description of the directional properties of the resulting wave field requires measuring devices capable of resolving details of directional wave spectra. Even a challenge by today's standards, this level of detail was not available in the measurements of one-dimensional frequency spectra reported by MPM62. Therefore, the assessment of wave spectra contaminated by crossing seas carrying significant energy at or above the observed spectral peak frequency in any particular event was not pursued in the original analysis made by M64.

Considering the encouraging results in modeling the directional properties of both winds and waves shown in Figs. 4 and 5, we assume that the directional distributions from the simulations described in the previous section provide a reliable approximation to the actual unknown directional distribution of measured spectra. Thus a reconstructed two-dimensional wave spectrum $\hat{E}(f, \theta)$ was obtained by multiplying the measured one-dimensional frequency spectrum $F(f)$ by the estimated directional distribution $\hat{D}(f, \theta)$, calculated with the wave model.

Figures 6 and 8 show plots of one-dimensional spectra and contour plots of the estimated 2D spectrum from events selected according to our synoptic criteria. Ex-

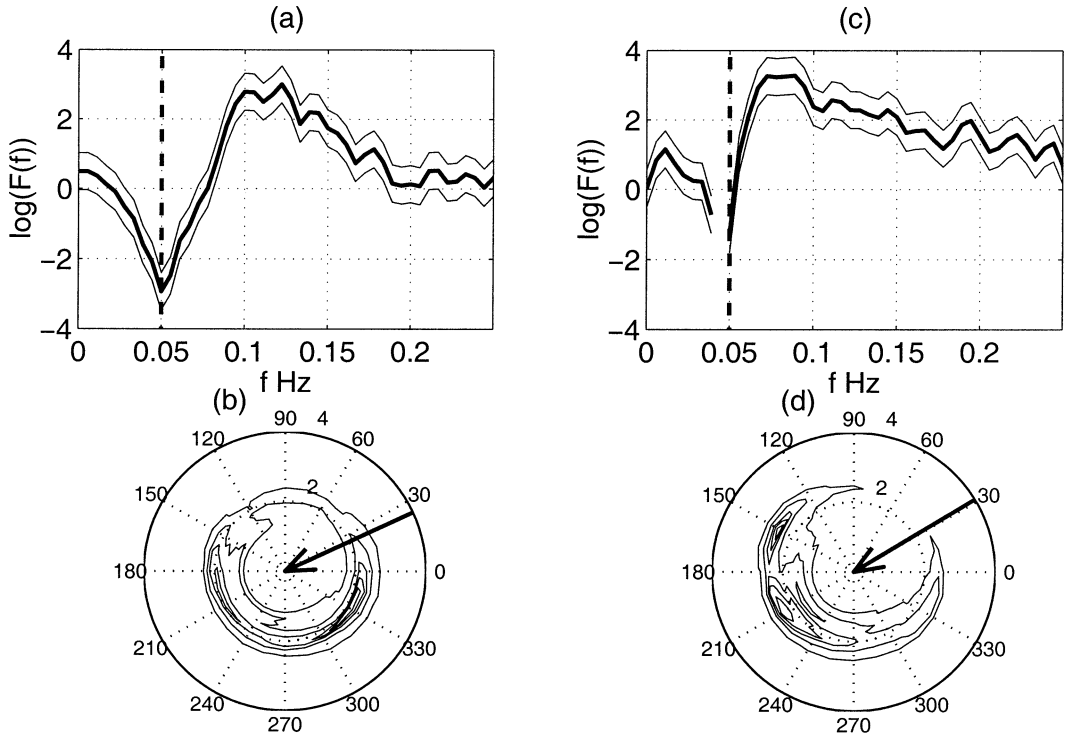

FIG. 6. Observed one-dimensional frequency spectra and associated 95% confidence limits at OWS (a) Alpha and (c) India, along with (b), (d) corresponding calculated directional distributions. Local wind directions are indicated by arrows in the lower panels. In (b) and (d), wave energies propagate outward from the center. Directions follow the WAVEWATCH III convention (i.e., east at 0°; north at 90°, etc.). Vertical dashed lines indicate swell separation scale in (a) and (c).

amples of spectra contaminated by crossing seas that were identified using the procedure outlined above are shown in Fig. 6 and Fig. 8. The wave spectrum shown in Figs. 6a and 6b was measured at OWS Alpha at 0300 UTC 23 May 1957. A secondary wave system from the southeast not associated with the local wind direction is clearly dominating the locally generated northeasterly wind sea. A snapshot of the NCEP–NCAR surface wind field 0300 23 May 1957, shown in Fig. 7a, indicates that a midlatitude storm generated a consistent northeasterly fetch over station Alpha but also exposed the station to waves generated by winds from the east-southeasterly sector.

Since the two crossing wave systems shown in Fig. 6b had similar peak frequencies (near $f = 0.11$ Hz and $f = 0.12$ Hz), they were not detected in the analysis made by M64. Depending on separation scales in both the frequency and the direction domains, the contributions of crossing wave fields to the total wave energy spectrum can be separated into individual subspectra. However, in this case the energy levels near frequencies at the spectral peak were relatively high within a broad range of directions, not allowing a clear distinction between spectra from the two predominant systems. This event and similar cases with clearly distinct but inseparable crossing wave systems were excluded from our reanalyzed database.

Other examples of a crossing-seas event that would go undetected in the analysis of one-dimensional frequency spectra are shown in Figs. 6c and 6d. This event was observed at station India at 0000 4 November 1955. The two crossing wave fields seen in Fig. 6d are associated with a midlatitude storm that produces divergent wind fetches near station Juliet, as indicated by the NCEP–NCAR surface wind fields shown in Fig. 7b. Although in this case the separation scale in terms of dominant frequencies between wave systems was relatively large (peak frequencies were $f = 0.07$ Hz and $f = 0.11$ Hz), the small angular separation between dominant directions of the crossing wave systems led to a superposition of spectral components in such a way that they did not produce distinctive individual peaks in the measured one-dimensional spectrum. This and similar events were excluded from the database of reanalyzed fully developed wind-sea spectra.

Whenever crossing wave systems were present but unambiguously distinct and separable, calculated directional distributions were used to correct observed spectra, allowing the elimination of energy associated with secondary systems that did not carry significant levels

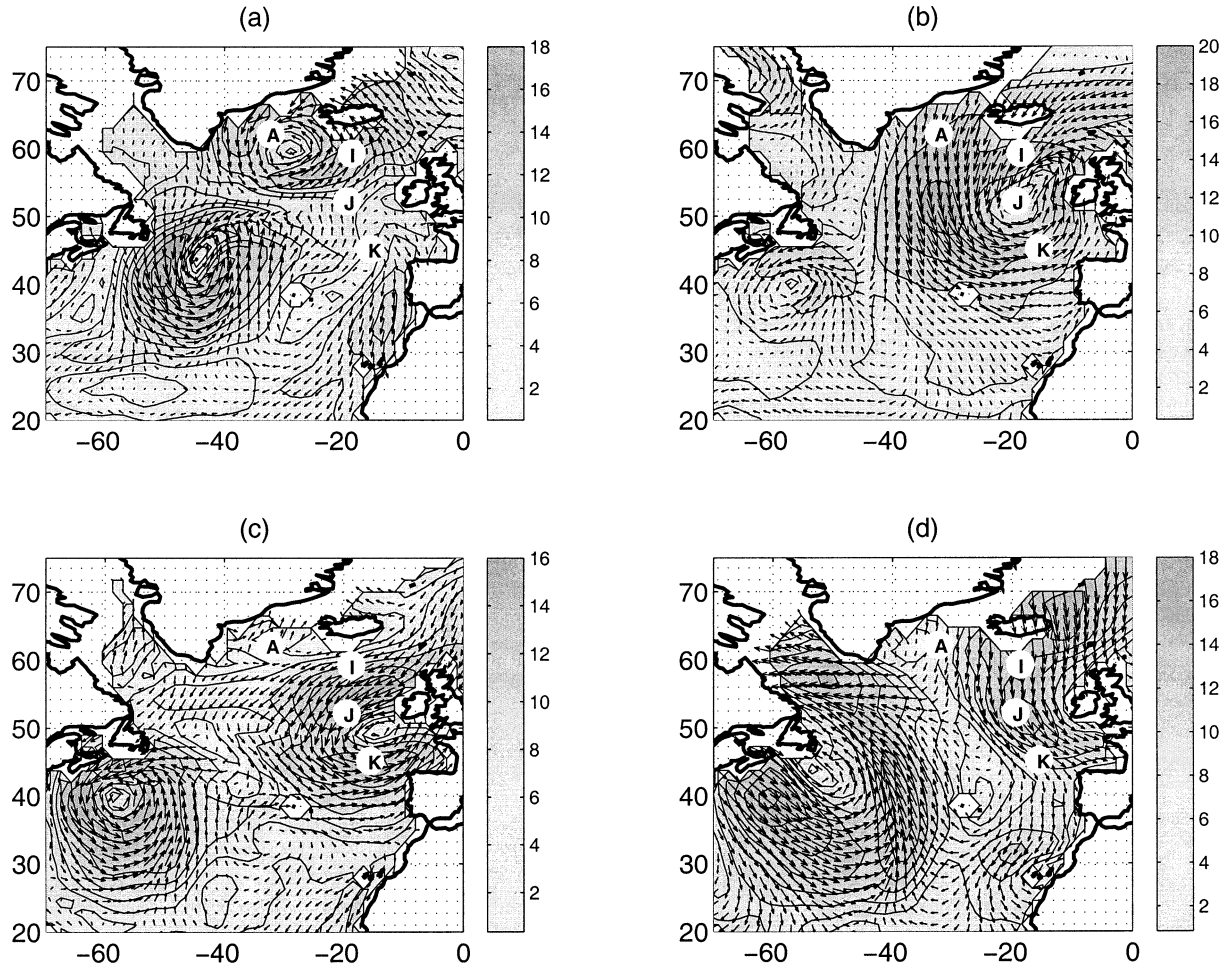

FIG. 7. NCEP–NCAR surface wind fields U_{10} from events associated with spectra shown in Figs. 6 and 8. The locations of OWS Alpha, India, Juliet, and Kappa are indicated.

of energy relative to the main fully developed wave system. These secondary systems were generally associated with dominant directions that were more than $\pm 90°$ from the primary wind-sea direction. An example is the spectrum shown in Figs. 8a and 8b, which is associated with an event observed at OWS Kappa at 1800 UTC 18 July 1955. The primary system was propagating from the northeast, while a secondary system is seen coming from the southwest. Associated NCEP–NCAR winds are shown in Fig. 7c. Our procedure for this event was to remove the spectral energy densities of wave components propagating toward the northeast, within the range corresponding to 0°–120° in Fig. 8b. This approach was also used in other cases with similar characteristics.

Table 1 presents the corrections made for crossing seas (CXS) to reanalyzed spectra selected for our final analysis in terms of percentage contribution to calculated values of E_{tot}. Cases retained in the database for further analysis were generally associated with values of CXS under 10%. Consequently, the sensitivity of the analysis carried out below to these corrections was considered negligible. Rejected cases in which crossing seas were either a significant contribution to E_{tot} or were associated with directions lying too close to the primary wind-sea direction are flagged in the last column of Table 2.

c. Removal of multiple-peaked spectra

A technique outlined in Rodriguez and Guedes-Soares (1999) was used to assist in the identification and removal of multipeaked spectra. The technique consists of displaying the variance of spectral estimates using a logarithmic transformation of spectral energy densities and then pinpointing ''true'' spectral peaks wherever the height of a spectral peak is above the confidence interval limits associated with the spectral estimates from other spectral ranges. Because of uncertainties in the high-frequency measurements of $F(f)$ in the MPM62 database, the analysis was restricted to a range of frequencies starting at the major peak with lowest frequency (excluding low-frequency swell) and trun-

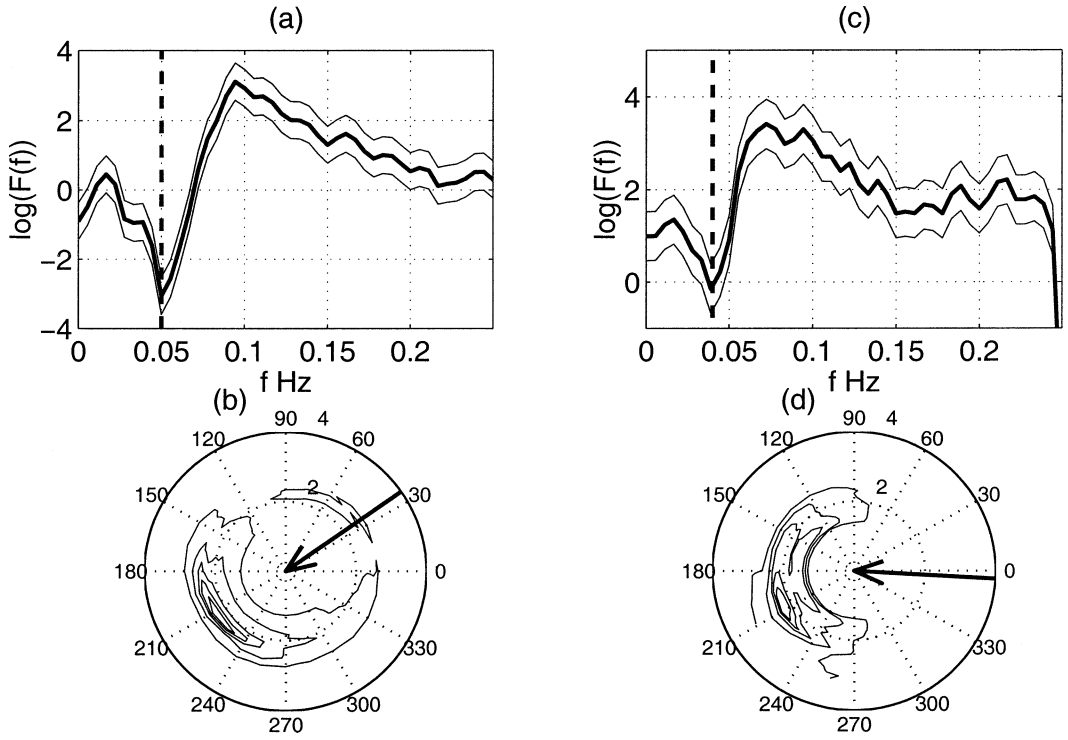

FIG. 8. As in Fig. 6 but for OWS Kappa.

cated at $f = 0.20$ Hz. Applying this criterion to observed fully developed spectra resulted in the rejection of six events indicated in Table 2, among which four were also rejected on the basis of contamination by crossing seas.

Examples of bimodal spectra rejected using the technique of Rodriguez and Guedes-Soares (1999) are shown Figs. 6c,d and 8c,d. The case shown in Fig. 6 was also rejected because of the presence of crossing seas, as discussed previously. The event shown in Fig. 8 was observed at station India at 2100 20 January 1958. Associated NCEP–NCAR surface winds are shown in Fig. 7d. In both cases, the secondary peaks are also confirmed by clear signatures in the calculated directional distributions.

d. Corrections for low-frequency swell

Low-frequency swell systems generated within both North and South Atlantic Oceans may be a source of contamination in fully developed sea spectra observed in the North Atlantic. The removal of swell contributions from measured spectra was made on the basis that these systems were generally associated with marked secondary spectral peaks centered at low frequencies, with a clearly distinguishable separation scale relative to the main spectral peak. Such separation scales are indicated in the one-dimensional frequency spectra shown in Figs. 6 and 8. After manually identifying these separation scales, corrections for low-frequency swell energy levels were made by simply setting spectral density levels at frequencies below the separation scale to zero. The percentage correction for swell is indicated in Table 1.

4. Results

After excluding spectra based on criteria for stationarity/homogeneity of winds, crossing seas, and multiple-peaked spectra, the database of fully developed sea spectra was reduced to the 29 events listed in Table 1. Figure 9 compares the 54 H_s values reported by M64 with 27 H_s values retained from the original database and recalculated after corrections for crossing seas and low-frequency swell contributions. Two new data points incorporated after our reanalysis of the MPM62 database are also indicated in Fig. 9.

Seeking increased statistical reliability and confidence, the available database was further refined in the following manner. First, unreliable high-frequency data were eliminated by replacing observed spectral densities within $0.25 \leq f \leq 1$ Hz with a diagnostic tail proportional to f^{-4}. The next step focused on reducing uncertainties associated with the individual observations of wind speeds and with the relatively low number of degrees of freedom—equal to 20—in each individual wave spectrum. This latter problem was found to be particularly critical. A preliminary verification of Eqs. (2) and (3), using H_s, E_{tot}, and f_p from the 29 selected

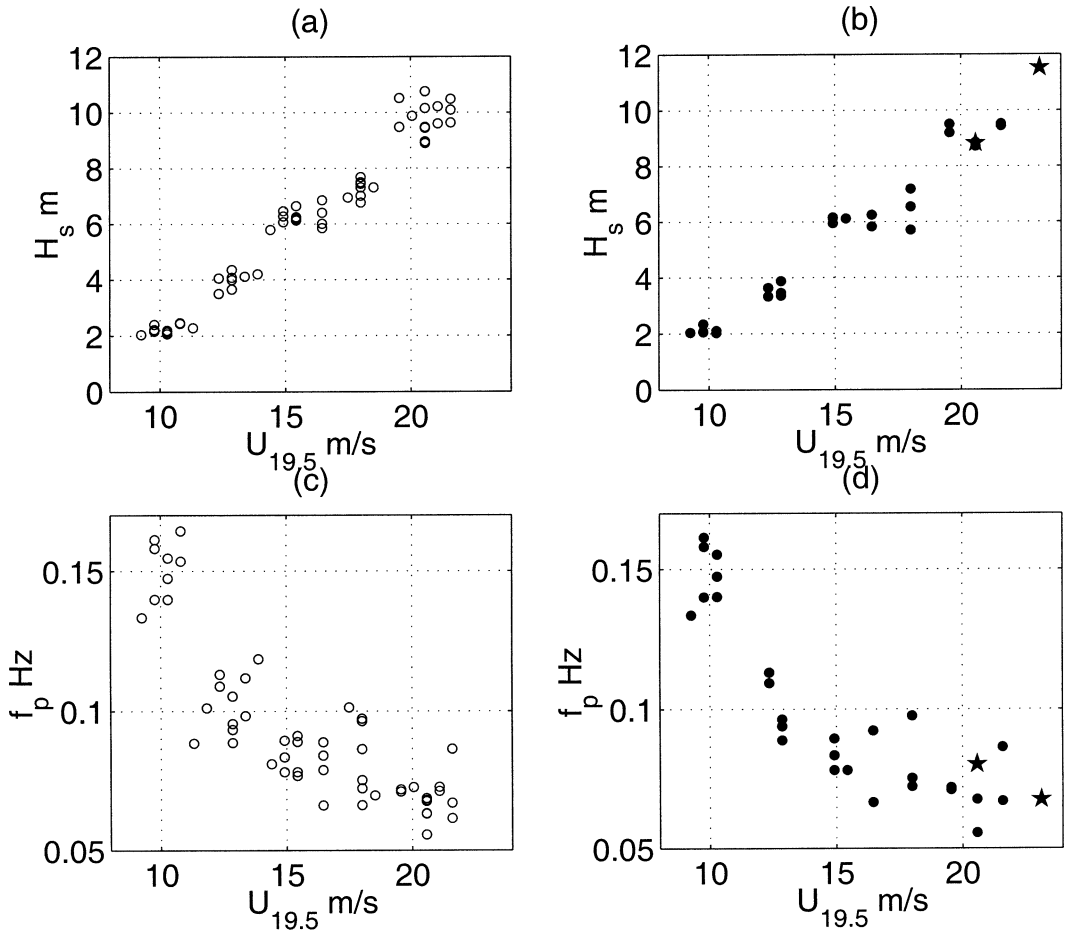

FIG. 9. Diagram showing H_s and f_p as a function of observed wind speeds $U_{19.5}$ before and after correction for crossing seas, multiple-spectral peaks, and/or low-frequency swell contamination: (a) H_s and (c) f_p from the original 54 cases used in the analysis made by M64; (b) H_s and (d) f_p from cases passing our quality-control criteria and used in the final analysis. Closed circles indicate cases taken from the original MPM62 database and stars indicate two newly selected events (see text in section 4).

events, indicated that the resulting confidence limits of measured wave spectra did not allow a statistically robust evaluation of the differential impact of using alternative reference wind speeds.

The shortcomings related to the reliability of wind speeds and to the confidence of wave spectral estimates were addressed simultaneously, after verifying that most of the 29 reanalyzed spectra could be grouped within 16 major events with conditions favorable to the occurrence of fully developed seas, according to our analysis of NCEP–NCAR surface winds. It was verified that 8 out of these 16 groups provided at least two observations of wave spectra and a recorded wind speed history extending mostly for 20–24 h prior to the wave measurements. The history of wind speed evolution in these eight groups, shown in Fig. 10, also allowed verifying the assumptions of stationarity of wind conditions, leading to the elimination of cases observed on 5 November 1955 because of variations of wind speeds greater than the acceptable margin of 20% relative to the mean in the 24-h period prior to the wave measurements.

Wind speeds from the remaining seven groups indicated in Table 1 were averaged, thus providing a more reliable and representative measure of the surface wind conditions associated with the occurrence of fully developed spectra. Pairs of spectra chosen from the latest times of each group were also averaged, providing mean spectral estimates of energy density with 40 degrees of freedom. The averaging of wind speeds and spectral estimates within groups provided an increase in statistical confidence, allowing a more accurate verification of the validity of Eqs. (2) and (3) using alternative reference wind speeds. It was reassuring to verify that the results obtained with these grouped data reproduced the values and general trends obtained when using all the 29 data points individually within acceptable statistical margins, except that the grouped data allowed greater statistical confidence. For this reason only results obtained from grouped data are presented below.

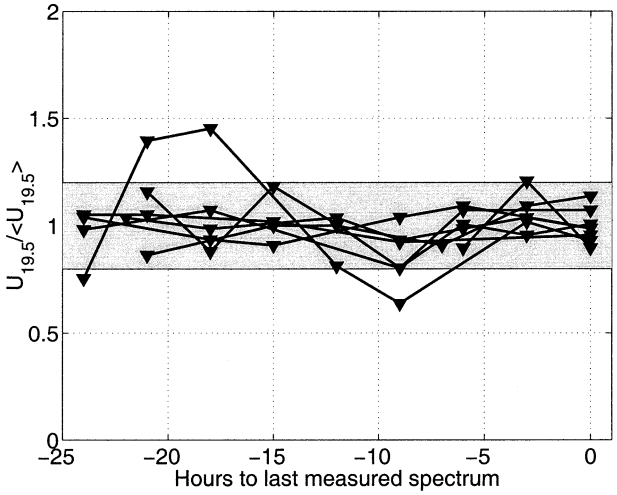

FIG. 10. History of wind speed evolution in hours prior to the last measured spectrum from eight groups of fully developed wind-sea events. The vertical scale indicates relative values to the mean wind speed of each group. The shaded area indicates a tolerance region of 20%.

a. Integrated parameters and similarity theory

Values of E_{tot}, H_s, and f_p calculated from seven grouped spectra and associated values of the candidate scaling wind speeds $U_0 = (U_{10}, u_*, U_{\lambda/2}$ or $U_r)$ were used to test the validity of the similarity theory relations in Eqs. (2) and (3). Parameters C_1 or C_2 and exponents n or l from Eq. (2) were estimated from these grouped data by fitting $\ln H_s$ or $\ln f_p$ to $\ln U_0$, respectively, using linear least squares. The relations were considered to be satisfied whenever (i) the differences between estimated exponents $\hat{n}$ or $\hat{l}$ and the expected values $n = 2$ or $l = -1$ were considered statistically negligible and (ii) the nondimensional parameters given by Eq. (3) were constant and statistically uncorrelated with the chosen scaling wind speed.

Estimates of f_p used in our analysis were obtained according to a weighted average method, as follows:

$$f_p = \frac{\int fF^4(f)\, df}{\int F^4(f)\, df}. \tag{16}$$

The statistical significance of results was inferred in terms of the confidence limits for the linear regression relations between $\ln H_s$ or $\ln f_p$ and $\ln U_0$, and for all dimensional and nondimensional variables. Confidence limits for the linear regression relations were obtained by assuming that individual data points were drawn from a nearly normally distributed population. Confidence limits for H_s were calculated following Young (1986). Unbiased estimates of f_p and their confidence limits were obtained following the procedure suggested by Young (1995), in association with Eq. (16).

Estimates for the confidence limits for nondimensional parameters, ϵ and ν, were based on Monte Carlo simulations of the variability of fetch-limited spectra reported by Young and Verhagen (1996). Their simulations were based on sharply peaked spectra with 112 degrees of freedom, which resulted in integral spectral parameters with similar number of degrees of freedom to spectral integrals associated with the ''flatter'' grouped spectra derived from our reanalyzed database of fully developed spectra. This is a consequence of the fact that the number of degrees of freedom of spectral integrals is strongly dependent on the spectral shape (Young 1986), increasing with decreasing spectral peakedness and vice versa.

Young and Verhagen (1996) used wind speed measurements averaged over 10-min periods to compute their nondimensional spectral integrals. Therefore, we assume that the statistical errors of their wind measurements would be comparable to those of wind speeds associated with our fully developed grouped spectra, which are mostly mean values of 5–10 measurements consisting of wind speeds averaged over 1 min, as reported by MPM62. Consequently, we chose the confidence limits for nondimensional spectral integrals calculated by Young and Verhagen (1996) to estimate the statistical uncertainty due to sampling variability in our fully developed grouped spectra.

1) SCALING WITH U_{10}

Values of wind speeds U_{10} and friction velocities u_* were derived from observations of $U_{19.5}$ reported in MPM62 using the ABL model of Liu et al. (1979). Group averages of U_{10} and u_* used observations obtained up to 24 h before the last measured wave spectrum of each group. Figure 11a shows values of H_s from average grouped spectra plotted against the associated average wind speed. The correlation coefficient between H_s and U_{10} is $r = 0.99$.

A regression line through the transformed variables $\ln H_s$ and $\ln U_{10}$, also shown in Fig. 11a, yields a relation $H_s = 0.025^{+0.039}_{-0.015} U_{10}^{2.01\pm0.35}$, where the $\pm$95% confidence intervals are indicated. The 95% confidence limits for H_s are also shown in Fig. 11. The estimated exponent $\hat{n} = 2.01$ is not different from the expected value $n = 2$ at the 95% confidence level.

Figure 11b shows the associated dependence between the observed nondimensional asymptote ϵ and U_{10}. Confidence limits for each group ϵ and for their mean value are also indicated in this figure. According to Eq. (3), these two variables should be uncorrelated, which implies a low value of the correlation coefficient r and also a linear regression line with slope approaching zero. These requirements are confirmed by the calculated correlation coefficient $r = -0.07$ and a regression slope of -1.36×10^{-5}, which is not significantly different from zero at the 95% confidence level. It is noteworthy

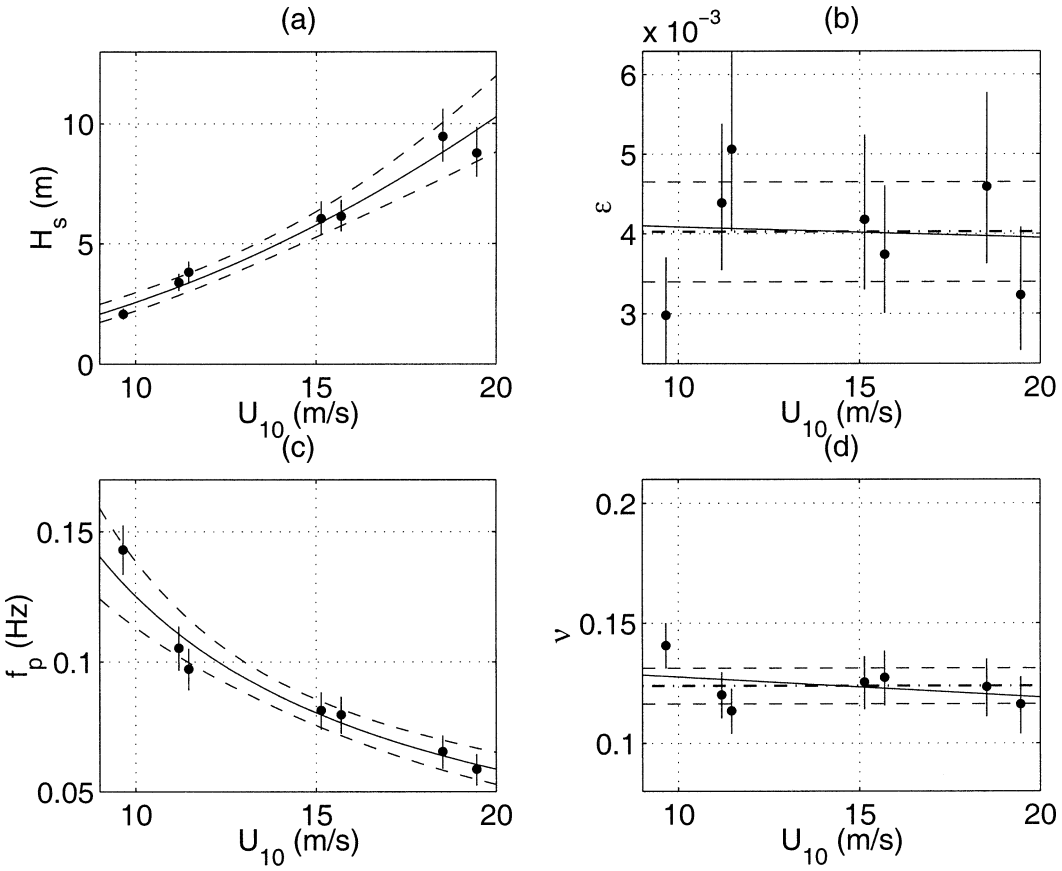

FIG. 11. Diagram showing the variation with U_{10} of (a) significant wave height H_s, (b) associated nondimensional energy ϵ, (c) peak frequency f_p, and (d) nondimensional peak frequency ν. All parameters are based on grouped spectra as described section 5. Confidence limits for dependent variables are shown as vertical bars.

that the confidence limits for ϵ mostly support the sample mean $\epsilon = 4.02 \times 10^{-3}$.

A similar analysis applied to f_p results in a correlation coefficient $r = -0.98$ between f_p and U_{10}. A linear regression between the transformed variables $\ln f_p$ and $\ln U_{10}$, shown in Fig. 11c, yields a relation $\hat{f}_p = 1.56^{+1.21}_{-0.74} U_{10}^{-1.09 \pm 0.24}$, where the estimated exponent $\hat{l} = -1.09$ satisfies similarity theory because it is statistically equivalent to the expected value of $l = -1$.

The resulting dependence between the asymptotic value of the nondimensional peak frequency ν and U_{10} is shown in Fig. 11d. Similarity theory is again satisfied as attested by a correlation level of $r = -0.30$ and a regression line with slope equal to 8.45×10^{-4}, which is not statistically different from zero at the 95% confidence level for the wind speed interval considered. Once more, the confidence limits for ν mostly support the sample mean $\nu = 1.23 \times 10^{-1}$.

The reanalyzed dataset, therefore, provides the following constants for the U_{10}-scaled asymptotes ϵ and ν:

$$\epsilon = (4.02 \pm 0.62) \times 10^{-3},$$
$$\nu = (1.23 \pm 0.08) \times 10^{-1}. \quad (17)$$

These resulting values of both U_{10}-scaled nondimensional asymptotes ϵ and ν are statistically equivalent to the asymptotes derived from the analysis made by M64 and PM64 [Eqs. (9) and (12)] at the 95% confidence level.

2) SCALING WITH u_*

Figure 12 shows diagrams of dimensional and nondimensional integral spectral parameters as a function of u_*, along with associated confidence limits for dependent variables. Despite the high correlation of $r = 0.98$ between H_s and u_*, a linear regression through $\ln H_s$ and $\ln u_*$ yields a relation $H_s = 13.42^{+2.96}_{-2.42} u_*^{1.62 \pm 0.29}$. The estimated exponent $\hat{n} = 1.62$ is statistically different from the exponent $n = 2$ predicted by similarity theory at the 95% confidence level.

Observed values of nondimensional total energy ϵ_* are significantly correlated with u_* ($r = -0.79$), also violating the requirements of similarity theory. Furthermore, a linear regression between these two variables yields a negative slope equal to -2.41×10^3, which is statistically different from zero at the 95%

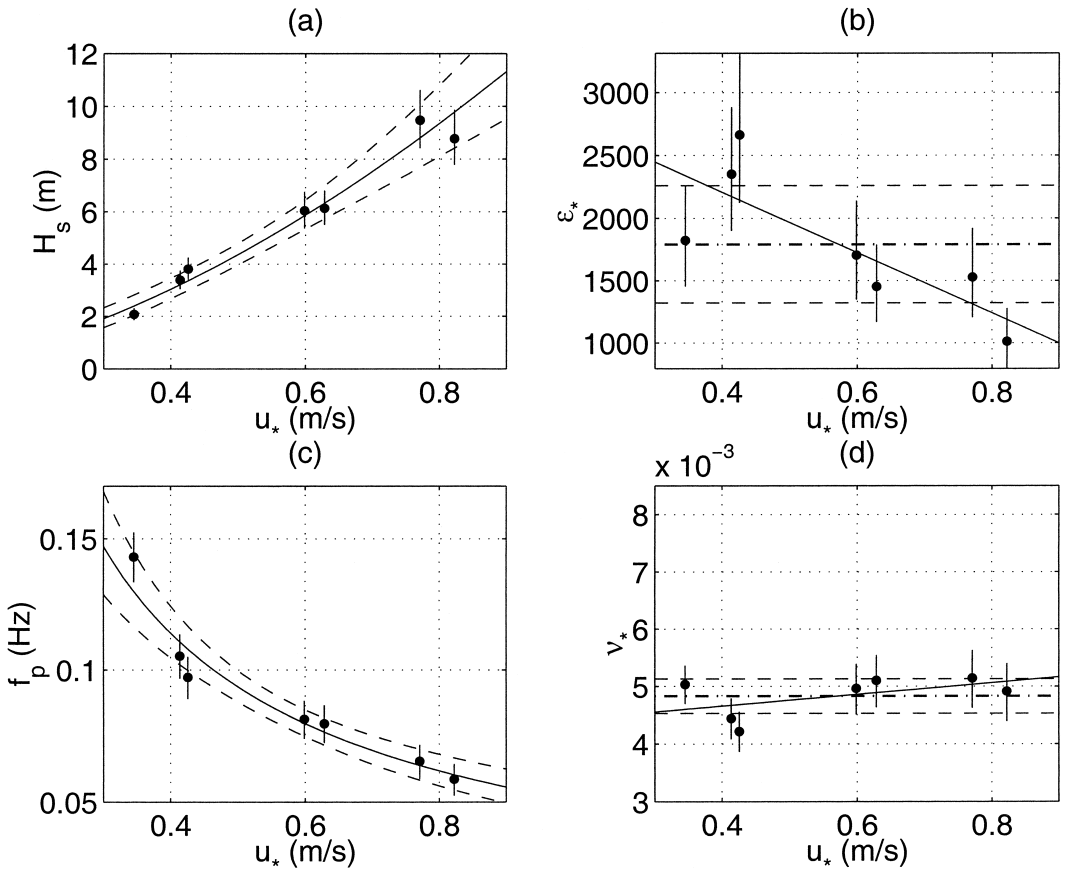

FIG. 12. Diagram showing the variation with u_* of (a) significant wave height H_s, (b) associated nondimensional energy ϵ_*, (c) peak frequency f_p, and (d) nondimensional peak frequency ν_*. All parameters are based on grouped spectra as described section 5. Confidence limits for dependent variables are shown as vertical bars.

confidence level and is also supported by the confidence limits for ϵ_*, as seen in Fig. 12b.

The requirements of similarity theory, nevertheless, are partially satisfied in statistical terms when f_p is scaled with u_*. The correlation between these two variables is high ($r = -0.98$) and the linear regression through $\ln f_p$ and $\ln u_*$, shown in Fig. 12c, yields $\hat{f_p} = (5.07^{+0.72}_{-0.64}) \times 10^{-2} u_*^{-0.88 \pm 0.19}$. The estimated exponent $\hat{l} = -0.88$ is lower but still statistically representative of the expected value $l = -1$ at the 95% confidence level. On the other hand, the correlation between nondimensional peak frequency values ν_* and u_* is relatively high ($r = 0.54$), as seen in Fig. 12d, and the linear regression line through $\ln f_p$ and $\ln u_*$ yields a positive slope equal to 1.14×10^{-3}, which is different from zero at the 95% confidence level.

Within the context of the database of fully developed seas events investigated in the present study, results for ϵ_* indicate that expressing the integrated spectral energy and scaling the associated nondimensional asymptote as a function of u_* yields relations that do not satisfy the requirements of similarity theory. Our results for ν_* suggest that this may also be the case for f_p and its associated u_*-scaled nondimensional asymptote, although in statistical terms these trends are not resolved.

Although of questionable validity in light of the results discussed above, average values of u_*-scaled nondimensional integral spectral parameters are given below for reference purposes and comparison with previously reported values. These are

$$\epsilon_* = (1.79 \pm 0.46) \times 10^3,$$
$$\nu_* = (4.83 \pm 0.30) \times 10^{-3}, \qquad (18)$$

which are significantly different to the values proposed by KHH, given by Eqs. (13) and (14).

3) SCALING WITH $U_{\lambda/2}$ AND U_r

For completeness, two other candidate scaling wind speeds were considered in our analysis. These were (i) the wind speed at a height corresponding to one-half of the wavelength of the dominant waves, $U_{\lambda/2}$, proposed by Donelan and Pierson (1987) and (ii) a dynamically scaled wind speed taken at a height that is linearly related to the wavelength of the spectral peak, U_r, pro-

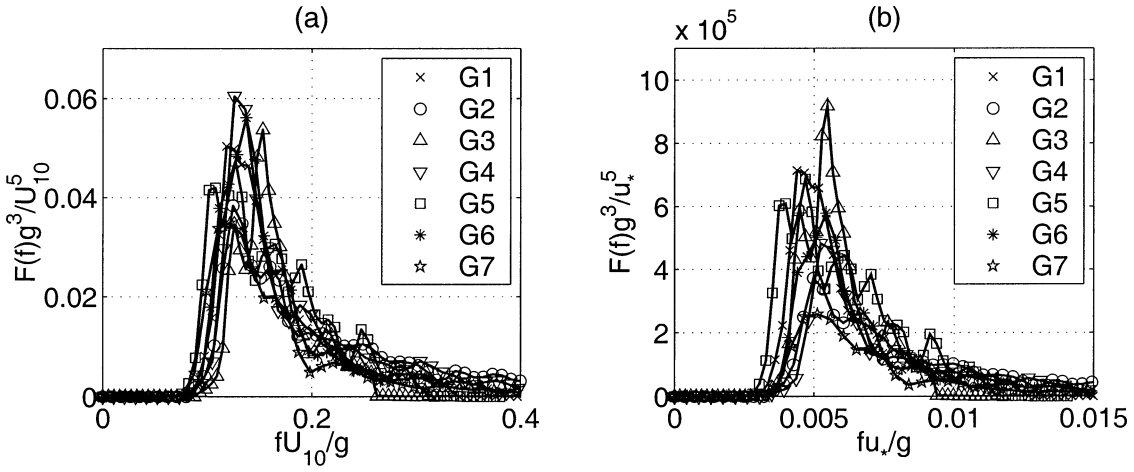

FIG. 13. Nondimensional grouped spectra from the reanalyzed database: (a) U_{10}-scaled spectra and (b) u_*-scaled spectra.

posed more recently by Resio et al. (1999). Both $U_{\lambda/2}$ and U_r were computed from neutrally stable values of U_{10} through (5); U_r was calculated following the iterative procedure outlined in Resio et al. (1999), with roughness length z_0 computed according to the model for the ABL of Liu et al. (1979).

Since these two scaling wind speeds are related to U_{10} through the same equations defining the logarithmic profile of the ABL that also defines u_*, it was not surprising to find that the trends of ϵ_* and ν_* with u_* were repeated for $U_{\lambda/2}$ and U_r. These trends, namely, (i) significant levels of correlation with the scaling wind speed and (ii) slopes of regression lines showing a functional dependence substantially beyond statistical confidence bounds, indicated that for the chosen dataset these two alternative scaling wind speeds do not provide robust relations for dimensional and nondimensional integral spectral parameters satisfying similarity theory.

b. Reanalyzed analytical spectra

Following common practice, one-dimensional spectra associated with fully developed conditions are expressed by analytical functions with one adjustable parameter α, also known as the Phillips constant, after Phillips (1958). This parameter determines the energy levels of the spectrum within the equilibrium range, which is well approximated by a power law in the form αf^{-n}. In this section we examine two alternative analytical one-dimensional spectral forms and their fit to measured spectra from our reanalyzed database.

Consistent with PM64 and other subsequent studies (e.g., the JONSWAP spectrum in Hasselmann et al. 1973, 1976), the first analytical expression to be examined is given by Eq. (7). The second analytical form used in our analysis follows the expression proposed by Donelan et al. (1985), as follows:

$$F(f) = \alpha g^2 (2\pi)^{-4} f^{-4} f_p^{-1} \exp\left[-\left(\frac{f}{f_p}\right)^{-4}\right]. \quad (19)$$

Equation (19) has a high-frequency spectral range proportional to f^{-4}, which has been supported by several field studies made since JONSWAP (e.g., Toba 1973; Kawai et al. 1977; Kahma 1981; Forristall 1981; Donelan et al. 1985).

The two forms Eqs. (7) and (19) were fitted to measured energy densities from the seven grouped spectra, which were made nondimensional with either $U_0 = U_{10}$ or $U_0 = u_*$ and normalized in terms of the ratio f/f_p. This gave $F'(f/f_p) = F(f/f_p)g^3/U_0^5$. We note that the technical limitations of the shipborne wave recorder used to collect the data reported by MPM62 required the elimination of spectral densities at frequencies greater than $f = 0.25$ Hz for fitting model to data. These nondimensional spectra are shown in Fig. 13.

Equations (7) and (19) were fitted to the normalized observations of spectral densities shown in Fig. 13 using linear least squares. Results are shown in Fig. 14. Analytical spectra of the form Eq. (7) fitted to U_{10}-scaled nondimensional spectral densities provided values of $\alpha = 9.52 \times 10^{-3}$, while fitting Eq. (7) to u_*-scaled spectra gave $\alpha = 11.76 \times 10^{-3}$. These parameter values provide analytical spectra that, although having slightly higher energy densities, are still consistent with the PM spectrum, which has $\alpha_{PM} = 8.10 \times 10^{-3}$, as seen in Fig. 14a. Values for α associated with the analytical form Eq. (19) derived from U_{10}-scaled nondimensional spectral densities were $\alpha = 6.15 \times 10^{-3}$, while the u_*-scaled spectra gave $\alpha = 6.84 \times 10^{-3}$. In both cases, these values of α for a spectral form with high-frequency tail proportional to f^{-4} were consistent with Donelan et al. (1985), who fitted a variant of Eq. (19) to fetch-limited data collected in Lake Ontario, Canada.

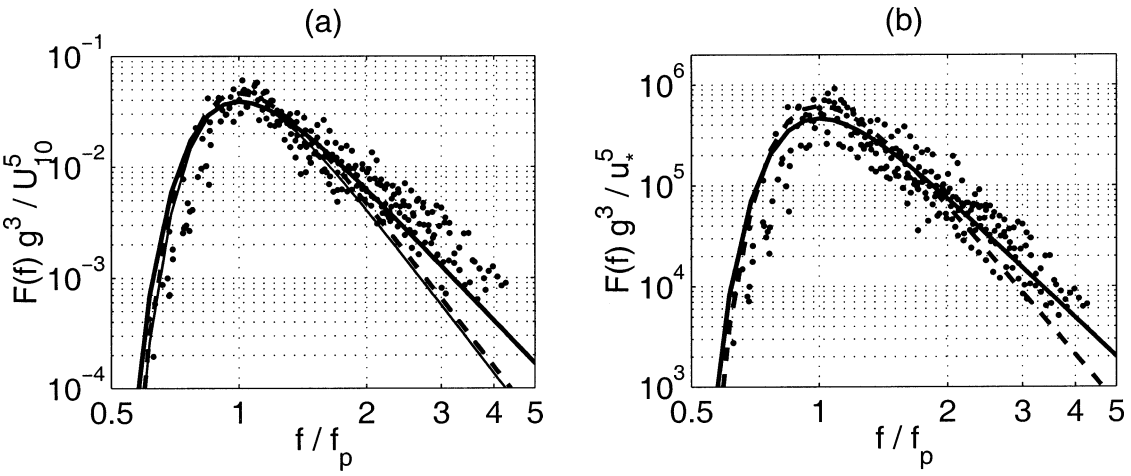

FIG. 14. Nondimensional analytical spectra fitted to the cloud of observed energy densities from the groups of selected fully developed wind-sea spectra. (a) Spectra are scaled with U_{10}; (b) the scaling is made with u_*. In each panel, the thick continuous line shows the fit of an analytical function with a spectral tail proportional to f^{-4}, while the broken line shows a spectral tail proportional to f^{-5}. In (a) the thin continuous line shows the PM64 analytical spectrum.

c. Relationship to wave-breaking threshold

Recently Banner et al. (2000) proposed a breaking threshold for deep water waves based on nonlinear hydrodynamics of wave groups. They reported a breaking threshold level for the significant steepness of the dominant waves of $\overline{s} = 0.055$, where $\overline{s} = H_p k_p/2$, H_p is the significant wave height computed from spectral components within $0.7 f_p < f < 1.3 f_p$ and k_p is the spectral peak wavenumber. It is of fundamental interest to review how our refined asymptotic spectra relate to the intuitive view that the dominant sea state corresponding to full development should imply zero wave breaking.

From the best-fit values for the parameter α in the analytical spectral forms proportional to f^{-5} and f^{-4}, by Eqs. (7) and (19), respectively, we calculated H_p and k_p. Because of the flat spectral peak and quadratic dispersion relationship between frequency and wavenumber, calculating k_p from the value for f_p estimated from the frequency spectrum results in an $O(10\%)$ overestimation of a value for k_p estimated directly from the equivalent wavenumber spectrum. To avoid this overestimation, we converted the analytical spectra from frequency to wavenumber space, obtaining thus a more accurate estimate of k_p.

With these considerations, we found $\overline{s} = 0.057$ for the analytical form with tail proportional to f^{-4} and $\overline{s} = 0.060$ for the analytical form with its spectral tail proportional to f^{-5}. The larger $\overline{s}$ in the latter case is due to a relatively higher concentration of energy around the peak for the spectrum with tail proportional to f^{-5}, resulting from the fact that both this and the analytical form proportional to f^{-4} had global energy levels fitted to the same data.

These estimates for the breaking threshold $\overline{s}$ from analytical spectra were verified against values for $\overline{s}$ calculated directly from the seven grouped spectra, after conversion of spectral densities from the frequency domain into their corresponding values in wavenumber domain. The result was a mean significant steepness $\overline{s} = 0.053$. In all cases, we may conclude that the limiting sea state is near or below the breaking threshold proposed by Banner et al. (2000). Hence the dominant waves for such sea states should not break, or break only rarely, a behavior consistent with our intuitive notions of full development.

5. Discussion

There are a number of issues arising from this study that warrant discussion. These include the most appropriate choice of wind velocity for scaling wave properties at full development, as well as the quality of the wind and wave data used by Pierson and Moskowitz in their pioneering work. Pierson and Moskowitz made a very careful selection and quality-control analysis of wind and wave data representative of fully developed conditions, designed to minimize the intrinsic limitations of the shipborne wind and wave measurements available for their study.

In this paper, we set out to refine the reliability of that dataset through the application of modern wind and wave hindcast technologies, thereby optimizing to the extent possible the data ensemble used by PM64. While our reanalysis confirmed much of the dataset selected by PM64 based on synoptic wind conditions, we were able to refine the wave quantities that are fundamental to the topic of fully developed seas by eliminating or correcting for spurious wave contributions, such as background swells or crossing wind seas. Although much reduced in size relative to the original database because of the elimination of unreliable data, the re-

analyzed dataset used in the present study is more representative of fully developed wind-sea conditions.

The issue of the most appropriate wind scaling velocity for characterizing the input from the wind to the wave field has been discussed in the literature over the past few decades, yet a strong consensus has yet to emerge. In this context, the findings of this study on the apparent robustness of U_{10} as the preferred scaling velocity in the full development asymptotes motivates further consideration.

The wind friction velocity u_* is the historically favored velocity scale because it characterizes the total wind stress and is independent of any scaling height. It sets the shear level in the assumed atmospheric boundary layer logarithmic mean wind profile that prescribes the wind input to the wave spectrum, according to shear flow instability theories that underlie the parameterization of wind input source functions used in spectral wind-wave models. However, u_* was seldom measured directly in early wave growth studies and, even then, it has potentially high intrinsic variability because of the frequent presence of large-scale organized ABL structures such as roll cells (e.g., see Chen et al. 2001, Fig. 8). Thus its use is complicated by significant observational uncertainties, as evidenced in all published determinations of the sea surface drag coefficient.

More recently, Donelan and Pierson (1987) and Resio et al. (1999) introduced other scaling velocities, $U_{\lambda/2}$ and U_r, respectively, to parameterize the spectral wind input to the wave field. However, $U_{\lambda/2}$ varies for each directional component in the wave spectrum. Therefore, extracting a single representative velocity scale for the resulting wind dependence of the entire wave spectrum at full development is not straightforward. In this context, the velocity scale associated with the spectral peak waves $U_{\lambda_p/2}$ seems to provide a reasonable nominal choice. Nevertheless, it is questionable whether $U_{\lambda_p/2}$ is a meaningful parameter in representing the whole evolution of the wave spectrum from early growth stages to full development since the spectral peak wavelength varies as the sea grows older. The same uncertainties arise when U_r is considered. Furthermore, the use of $U_{\lambda/2}$ seems to be limited to a height of around 20 m, above which the ABL becomes dominated by Coriolis effects and convection and might not be expected to be closely related to the wind-wave field (M. A. Donelan 2001, personal communication).

Another possibility is the historical choice of U_∞, the wind velocity at the outer edge of the ABL, as specified by Kitaigorodskii (1973): U_∞ is seldom measured; hence a surrogate scaling velocity is needed that is more accessible to measurement. As discussed by Pierson (1964), this role has been filled by the wind speed at a fixed mean level above the sea surface ($U_{19.5}$, U_{10}, etc.) in combination with the adoption of a logarithmic ABL profile adjusted for atmospheric stability effects. The 10-m height wind velocity U_{10} has been the most popular historical choice as a reference velocity owing to its relative ease of measurement. Clearly, this choice of scaling wind velocity is arbitrary with respect to wave scale, but our study indicates that for the fully developed dataset used in our analysis, it appears to provide the most self-consistent representative wind speed scale in the integral parameter correlations for asymptotic sea states.

We refrain from speculation as to the underlying justification for the results presented above and leave the resolution of this issue to future studies of fully developed sea states based on more comprehensive datasets that are now potentially available with modern measurement capabilities. Such studies would seek to minimize the unknown influence on our conclusions from observational errors associated with the shipboard wind and wave measurements underlying the present investigation.

6. Summary and concluding remarks

The present study is an effort toward increasing confidence in the available measurements of fully developed wind waves. Our objectives were (i) to verify the validity of asymptotic nondimensional parameters based on different scaling wind speeds and (ii) to review the asymptotic benchmark limits adopted by the wind-wave modeling community. The focus of this study was on a review of the results reported by Moskowitz (1964) and Pierson and Moskowitz (1964), which provide an important asymptote in the validation of numerical models under idealized fetch- and duration-limited conditions.

A reanalysis of 460 observations of wave spectra used originally by Moskowitz (1964) and Pierson and Moskowitz (1964) is made. This reanalysis was based on criteria for the stationarity of wind fields and for the levels of contamination for crossing seas and background swell. A total of 27 events with atmospheric conditions not satisfying minimum synoptic criteria or showing evidence of significant contamination by swell or crossing wind seas was eliminated. Two new events were added to the original dataset on the basis of reanalyzed wind fields.

These 29 retained spectra were corrected for contamination by crossing seas and swell. Seven pairs of spectra and associated wind speed histories were then finally selected and used to investigate the validity of similarity theory using different scaling winds and to rederive the full-development asymptotes. Our results indicated that

1) values of U_{10}-scaled nondimensional asymptotes were statistically equivalent to those from the original analysis made by M64 and PM64;
2) the parameterization of integral spectral parameters and the scaling of associated nondimensional asymptotes with U_{10} yields relations that conform to Kitaigorodskii's similarity theory;
3) values of u_*-scaled nondimensional asymptotes were

statistically different to those from previous values proposed by KHH;

4) integral spectral parameters and nondimensional asymptotes scaled by the friction velocity u_* yield relations that do not satisfy the requirements of similarity theory. Similar trends were found when two other alternative scaling wind speeds, $U_{\lambda/2}$ and U_r, were used.

We conclude that for the chosen dataset only scaling with U_{10} provides statistically robust relations for dimensional and nondimensional parameters satisfying Kitaigorodskii's similarity theory.

Reanalyzed spectra were also used to derive parameter values of analytical functions representing one-dimensional fully developed spectra. Two analytical forms with energy densities at the spectral tail proportional to f^{-4} and f^{-5} were fitted to both U_{10}- and u_*-scaled nondimensional spectra. The analytical spectral form with high-frequency tail proportional to f^{-4} provided a better fit to the data than the form with tail proportional to f^{-5}. Parameters associated with both analytical forms were consistent with values proposed by Donelan et al. (1985) and Pierson and Moskowitz (1964), respectively.

Last, we review how our refined asymptotic spectra relate to the intuitive view that the dominant sea state corresponding to full development should imply zero wave breaking. For this purpose, we use a recently proposed breaking threshold for deep water waves reported by Banner et al. (2000). Our analysis of analytical and measured spectra provided values for this parameter that were very near or below the observed breaking threshold. Hence, we conclude that the dominant waves for such sea states should not break, or break only rarely, a behavior consistent with our intuitive notions of fully developed wind seas.

Acknowledgments. We are very grateful to Dr. Willard Pierson for providing reports containing spectra used in the original Pierson–Moskowitz studies of fully developed seas. Dr. Pierson, Mr. Lionel Moskowitz, Dr. Hendrik Tolman, and anonymous referees also provided extensive material for discussion, technical support, and encouragement that are gratefully acknowledged. We thank Mr. Andre G. Almeida for digitizing the observed spectra from the Pierson–Moskowitz reports and the School of Civil Engineering of the Australian Defence Force Academy for operational support during the preparation and realization of this study. J.H.G.M. Alves gratefully acknowledges the support of the Conselho Nacional de Desenvolvimento Cientifico e Tecnologico (CNPq), Brazil, through the PhD scholarship GDE 200.241/96-6, and fellowships granted by the Inter-American Institute for Climate Research (IAI-SACC) and by The University of New South Wales. Michael L. Banner and I. R. Young gratefully acknowledge the support of the Australian Research Council and the U.S. Office of Naval Research. This paper is dedicated to the memory of our esteemed colleague Willard J. Pierson, in recognition of his very substantial scientific contributions to the field of surface processes.

REFERENCES

Banner, M. L., and I. R. Young, 1994: Modeling spectral dissipation in the evolution of wind waves. Part I: Assessment of existing model performance. *J. Phys. Oceanogr.,* **24,** 1550–1571.

——, A. Babanin, and I. R. Young, 2000: Breaking probability for dominant waves on the sea surface. *J. Phys. Oceanogr.,* **30,** 3145–3160.

Bretschneider, C. L., 1966: Wave generation by wind, deep and shallow water. *Estuary and Coastline Hydrodynamics,* Eng. Soc. Monogr., McGraw-Hill Book Co., 744 pp.

CERC, 1984: *Shore Protection Manual.* Vol. 1. U. S. Army Coastal Engineering Research Center, Dept. of the Army Corps of Engineers, 180 pp.

Chen, W., M. L. Banner, E. J. Walsh, J. B. Jensen, and S. Lee, 2001: The Southern Ocean Waves Experiment. Part II: Sea surface response to wind speed and wind stress variations. *J. Phys. Oceanogr.,* **31,** 174–198.

Cote, L. J., and Coauthors, 1960: The directional spectrum of a wind-generated sea as determined from data obtained by the Stereo Wave Observation Project. New York University College of Engineering Meteorological Papers, 1–88.

Darbyshire, J., 1959: A further investigation of wind generated waves. *Dtsch. Hydrogr. Z.,* **12,** 1–13.

Davidan, I. N., 1996: New results in wind-wave studies (in Russian). *Meteor. Hydrol.,* **4,** 65–72.

Donelan, M. A., and W. J. Pierson, 1987: Radar scattering and equilibrium ranges in wind-generated waves with applications to scatterometry. *J. Geophys. Res.,* **92,** 4971–5029.

——, J. Hamilton, and W. H. Hui, 1985: Directional spectra of wind-generated waves. *Philos. Trans. Roy. Soc. London,* **A315,** 509–562.

——, M. Skafel, H. Graber, P. Liu, D. Schwab, and S. Venkatesh, 1992: On the growth rate of wind-generated waves. *Atmos.–Ocean,* **30,** 457–478.

Ebuchi, N., H. Kawamura, and Y. Toba, 1992: Growth of wind waves with fetch observed by the GEOSAT altimeter in the Japan Sea under winter monsoon. *J. Geophys. Res.,* **97,** 809–819.

Ewing, J. A., and A. K. Laing, 1987: Directional spectra of seas near full development. *J. Phys. Oceanogr.,* **17,** 1696–1706.

Forristall, G. Z., 1981: Measurements of a saturation range in ocean wave spectra. *J. Geophys. Res.,* **86,** 8075–8084.

Glazman, R. E., 1994: Surface waves at equilibrium with a steady wind. *J. Geophys. Res.,* **99** (C3), 5249–5262.

——, and S. H. Pilorz, 1990: Effects of sea maturity on satellite altimeter measurements. *J. Geophys. Res.,* **95** (C3), 2587–2870.

Hanson, J. L., and O. M. Phillips, 1999: Wind sea growth and dissipation in the open ocean. *J. Phys. Oceanogr.,* **29,** 1633–1648.

Hasselmann, K., and Coauthors, 1973: Measurements of wind-wave growth and swell decay during the Joint North Sea Wave Project (JONSWAP). *Dtsch. Hydrogr. Z.,* **8** (12); (Suppl. A), 1–95.

——, D. B. Ross, P. Müller, and W. Sell, 1976: A parametric wave prediction model. *J. Phys. Oceanogr.,* **6,** 200–228.

Hersbach, H., 1998: Application of the adjoint of the WAM model to inverse wave modeling. *J. Geophys. Res.,* **103** (C5), 10 469–10 487.

Holthuijsen, L. H., 1983: Observations of the directional distribution of ocean-wave energy in fetch-limited conditions. *J. Phys. Oceanogr.,* **13,** 191–207.

Hwang, P. A., D. W. Wang, E. J. Walsh, W. B. Krabill, and R. N. Swift, 2000: Airborne measurements of the wavenumber spectra of ocean surface waves. Part II: Directional distribution. *J. Phys. Oceanogr.,* **30,** 2768–2787.

Janssen, P. A. E. M., G. J. Komen, and W. J. P. de Voogt, 1987:

Friction velocity scaling in wind-wave generation. *Bound.-Layer Meteor* **38,** 29–35.
Kahma, K. K., 1981: A study of the growth of the wave spectrum with fetch. *J. Phys. Oceanogr.,* **11,** 1503–1515.
——, and C. J. Calkoen, 1992: Reconciling discrepancies in the observed growth of wind-generated waves. *J. Phys. Oceanogr.,* **22,** 1389–1405.
Kalnay, E., and Coauthors, 1996: The NCEP/NCAR 40-Year Reanalysis Project. *Bull. Amer. Meteor. Soc.,* **77,** 437–471.
Kawai, S., K. Okada, and Y. Toba, 1977: Field data support of three-seconds power law and $gu_*\sigma^{-4}$ spectral form for growing wind waves. *J. Oceanogr. Soc. Japan,* **33,** 137–150.
Kitaigorodskii, S. A., 1962: Applications of the theory of similarity to the analysis of wind-generated wave motion as a stochastic process. *Bull. Acad. Sci. USSR Geophys. Ser.,* **1,** 105–117.
——, 1973: *The Physics of Air–Sea Interaction.* Israel Program for Scientific Translations Ltd., 239 pp.
Komen, G. J., S. Hasselmann, and K. Hasselmann, 1984: On the existence of a fully-developed wind-sea spectrum. *J. Phys. Oceanogr.,* **14,** 1271–1285.
——, L. Cavaleri, M. A. Donelan, K. Hasselmann, S. Hasselmann, and P. A. E. M. Janssen, 1994: *Dynamics and Modelling of Ocean Waves.* Cambridge University Press, 532 pp.
Lindau, R., 1995: A new Beaufort equivalent scale. *Proc. Int. COADS Workshop,* Kiel, Germany, Institut für Meereskunde Kiel and NOAA, 232–252.
Liu, P. C., and D. B. Ross, 1980: Airborne measurements of wave growth for stable and unstable atmospheres in Lake Michigan. *J. Phys. Oceanogr.,* **10,** 1842–1853.
Liu, W. T., and W. Tang, 1996: Equivalent neutral wind. JPL Publ. 96-17, 8 pp.
——, K. B. Katsaros, and J. A. Businger, 1979: Bulk parameterization of air–sea exchanges in heat and water vapor including the molecular constraints at the interface. *J. Atmos. Sci,* **36,** 1722–1735.
Mitsuyasu, H., F. Tasai, T. Suhara, S. Mizuno, M. Okhuso, T. Honda, and K. Rikiishi, 1975: Observations of the directional spectrum of ocean waves using a cloverleaf buoy. *J. Phys. Oceanogr.,* **5,** 750–760.
Moskowitz, L., 1964: Estimates of the power spectrums for fully-developed seas for wind speeds of 20 to 40 knots. *J. Geophys. Res.,* **69,** 5161–5179.
——, W. J. Pierson, and E. Mehr, 1962: Wave spectra estimated from wave records obtained by the OWS Weather Explorer and the OWS Weather Reporter. Parts 1, 2 and 3. Tech. Rep., U. S. Naval Oceanographic Office, New York University, approx. 58 pp.
Phillips, O. M., 1958: The equilibrium range in the spectrum of wind-generated ocean waves. *J. Fluid Mech.,* **107,** 465–485.
Pierson, W. J., 1964: The interpretation of wave spectrum in terms of the wind profile instead of the wind measured at a constant height. *J. Geophys. Res.,* **69,** 5191–5203.
——, and L. Moskowitz, 1964: A proposed spectral form for fully developed wind seas based on the similarity theory of A. A. Kitaigorodskii. *J. Geophys. Res.,* **69,** 5181–5190.
——, G. Neumann, and R. James, 1955: Practical methods for observing and forecasting ocean waves by means of wave spectra and statistics. H.O. Publ. 603, U. S. Navy Hydrographic Office, 284 pp.
Resio, D. T., V. R. Swail, R. E. Jensen, and V. J. Cardone, 1999: Wind speed scaling in fully developed seas. *J. Phys. Oceanogr.,* **29,** 1801–1811.
Ris, R. C., 1997: Spectral modelling of wind waves in coastal areas. *Communications on Hydraulic and Geotechnical Engineering,* Technical University of Delft Rep. 97-4, 160 pp.
Rodriguez, G., and C. Guedes-Soares, 1999: A criterion for the automatic identification of multimodal sea wave spectra. *Appl. Ocean Res.,* **21,** 329–333.
Schneggenburger, C., 1998: Spectral wave modelling with nonlinear dissipation. Ph.D. dissertation, GKSS-Forschungszentrum Geesthacht GmbH, Hamburg, Germany, 117 pp.
Silvester, R., 1974: *Coastal Engineering.* Vol. 1. Elsevier Scientific Publishing, 457 pp.
Smith, S. D., 1980: Wind stress and heat flux over the ocean in gale force winds. *J. Phys. Oceanogr.,* **10,** 709–726.
Sverdrup, H. V., and W. H. Munk, 1947: Wind sea and swell: Theory of relation for forecasting. H. O. Publ. 601, U.S. Navy Hydrographic Office, 44 pp.
SWAMP Group, 1985: *Ocean Wave Modeling.* Plenum Press, 256 pp.
Taylor, P. K., and M. J. Yelland, 2001: The dependence of sea surface roughness on the height and steepness of the waves. *J. Phys. Oceanogr.,* **31,** 572–590.
Toba, Y., 1973: Local balance in the air–sea boundary process. *J. Oceanogr. Soc. Japan,* **29,** 209–220.
Tolman, H. L., 1999: User manual and system documentation of WAVEWATCH-III version 1.18. NOAA/NWS/NCEP/OMB Tech. Note 166, 110 pp.
Walsh, E. J., D. W. Hancock III, D. E Hines, R. N. Swift, and J. F Scott, 1989: An observation of the directional wave spectrum evolution from shoreline to fully developed. *J. Phys. Oceanogr.,* **19,** 670–690.
Wu, J., 1982: Wind-stress coefficients over the sea surface from breeze to hurricane. *J. Geophys. Res.,* **87** (C12), 9704–9706.
Young, I. R., 1986: Probability distribution of spectral integrals. *J. Waterw., Ports, Coastal Ocean Eng.,* **112,** 338–341.
——, 1995: The determination of confidence limits associated with estimates of the spectral peak frequency. *Ocean Eng.* **22,** 669–686.
——, and L. A. Verhagen, 1996: The growth of fetch-limited waves in water of finite depth. Part I: Total energy and peak frequency. *Coastal Eng.* **28,** 47–78.